Technische Universität München

Fakultät für Chemie / Fachgebiet für Elektronenmikroskopie

Early stages of crystallization of lumazine synthase from *Bacillus subtilis*

Nikolaus Neumaier

Vollständiger Abdruck der von der Fakultät für Chemie der Technischen Universität München zur Erlangung des akademischen Grades eines

Doktors der Naturwissenschaften

genehmigten Dissertation.

Vorsitzender: Univ.-Prof. Dr. Dr. A. Bacher

Prüfer der Dissertation:

1. Univ.-Prof. Dr. S. Weinkauf
2. Ass. Prof. P.G. Vekilov, Ph.D.
   Univ. of Houston / USA

Die Dissertation wurde am 25.04.2005 bei der Technischen Universität München eingereicht und durch die Fakultät für Chemie am 31.05.2005 angenommen.

Acknowledgements

First I would like to thank Prof. Dr. Sevil Weinkauf for giving me the oportunity to work in the fascinating field of crystal growth and for her excellent supervision, encouragement, for her trust in me and in my work. I am also grateful to her for providing the international atmosphere at the institute: encouraging her students to attend conferences, meetings and summer schools and to cooperate with other research groups.

I would like to express my gratitude to Prof. Dr. Peter Vekilov and Dr. Olga Gliko for the inspiring cooperation and the hospitality and nice time I spent in Houston.

I would also like to express my appreciation to Dr. Lidia Rodríguez Fernández for introducing me into the field of protein crystallization, the valuable suggestions regarding experimental work and all the fruitful discussions.

Many thanks to Dr. Johannes Scheuring for his help in biochemistry and a never ending supply of coffee and to Dr. Marianne Hanzlik for her help with electron microscopy and many thanks to Marion Junker, Dr. Nathalie Braun and everybody in our group for the cordial atmosphere.

Many thanks to all my friends who never lost confidence in me and always tried to convince me that there exists a life outside the lab.

Finally, I would like to thank my parents and my sister for their support and love during all these years.

Abstract

The subject of this study was the analysis of solubility, particle interactions and aggregation behavior of lumazine synthase from *Bacillus subtilis*. Lumazine synthase crystallizes in sodium/potassium phosphate buffer, pH 8.7. Contrary to the decrease in solubility with increasing salt concentration, the osmotic second virial coefficient remains almost constant and reveals the same slight attractive interactions under storage and crystallization conditions.

In search of protein clusters that are involved in and accompany crystal nucleation, supersatured solutions of lumazine synthase were studied by dynamic light scattering and cryo transmission electron microscopy. As predicted by the classical nucleation theory, increased supersaturation facilitated the nucleation of crystals. This was accompanied by an increased detection of aggregates until the light scattering spectra were dominated by uncorrelated intensity fluctuations caused by a few but large aggregates, presumably microcrystals. Electron micrographs of supersaturated solutions showed network-like assemblies of lumazine synthase molecules and in addition lumazine synthase clusters with a linear arrangement.

Even in supersaturated solutions of lumazine synthase where no nucleation took place, aggregates were detected by dynamic light scattering. In connection with atomic force microscopy studies carried out in the laboratory of Prof. Peter Vekilov at the University of Houston, Department of Chemical Engineering, Texas, USA, these aggregates were identified as dense liquid droplets of lumazine synthase that are metastable in respect to the original and the crystal phase. At low supersaturations these liquid droplets are the only source of new crystal growth layers.

Contents

List of Tables

List of Figures

Index of Abbreviations

APS	ammonium persulphate
BMV	brome mosaic virus
cP	centi-Poise = 10^{-3} Pa s
DLS	dynamic light scattering
DTT	dithiothreitol
DMS	polydimethylsiloxane
EDTA	ethylenediaminetetraacetic acid
eq	equation
fcc	face centered cubic
fig	figure
IPTG	isopropyl-β-D-thiogalactopyranosid
NMR	nuclear magnetic resonance
OD	optical density
PEG	polyethylene Glycol
pI	isoelectric point
PMSF	phenylmethylsulphonyl fluoride
rpm	rounds per minute
SDS-PAGE	sodium dodecylsulfate polyacrylamide gel electrophoresis
SLS	static light scattering
T	temperature
t	time
TEM	transmission electron microscopy
TEMED	N,N,N',N'-tetramethylethylenediamine
Tris	tris(hydroxymethyl)aminomethane

1 Introduction

1.1 Protein crystallization

Protein crystallization is the process of segregation of a solid phase with short- and long-range order from an aqueous protein solution that is brought into supersaturation (McPherson, 1999; Pimpinelli and Villain, 1998).

Detailed knowledge of the three-dimensional structure at high resolution is essential to understand the molecular function of biological macromolecules and hence, to develop novel drugs and pharmaceutical products and to engineer proteins with improved properties (Blundell et al., 2002; Davis et al., 2003). The periodicity in position and orientation of the macromolecules in 3-dimensional crystals is utilized in x-ray crystallography to determine the molecular structure at atomic-resolution by analyzing the x-ray diffraction pattern (Drenth, 1994; McPherson, 2003). Nuclear magnetic resonance is widely used to determine dynamics and structure of proteins in solution. However, it is limited to proteins with a molecular weight of less than 40 kDa. Electron crystallography and tomography provide information at near-atomic resolution of membrane proteins, macromolecular complexes and subcellular assemblies.

Despite the vast effort that has been expended on structural proteomics (Sali et al., 2003) only for a small fraction of expressed and purified proteins the structure could be solved at atomic-resolution by x-ray crystallography (Chayen, 2004). Either the proteins could not be crystallized or the crystals yielded only poorly resolved diffraction patterns and the amino acid sequence could not be fitted into the electron density map.

On one hand, diffraction resolution is limited by the conformational flex-

ibility of macromolecules, the variability in packing and the inhomogeneity of large assemblies like virions (Malkin and McPherson, 2002). In addition, the regular arrangement in crystals is disturbed by conventional defects that are observed in crystals of small molecules as well, like point defects arising from vacancies and incorporation of impurities, dislocations, stacking faults and grain boundaries (Chernov, 1997; McPherson et al., 2003, 1996). Furthermore, rotational disorder may lead to low resolution or complete absence of diffraction pattern. Braun et al. (2000) showed by electron microscopy of freeze-etched and silver decorated surfaces of lumazine synthase crystals that rotational disorder of lumazine synthase molecules preferentially occurs near relief perturbations.

It is not known which of these defects have the most aggravating impact on diffraction resolution. However, any defects present at the initial stages of crystallization cannot heal at later stages of crystal growth because of the lack of plasticity, i.e. mobility of the defects (Chernov, 2003).

1.1.1 Particle interactions

The problem of assembling of macromolecules into crystals with high specificity in position and orientation is related to the problem of macromolecular interactions and molecular recognition in solutions.

Interactions are driven by different forces including hard-sphere, electrodynamic (London dispersion / van der Waals) and electrostatic forces (Israelachvili, 1985). Hard-sphere potential reflects the fact that macromolecules cannot interpenetrate. Dispersion forces are short ranged and attractive but negligible compared to the electrostatic forces. The main contribution to the

latter is the Coulomb repulsion that depends on the charge of the macromolecules and ionic strength as described by the Derjaguin-Landau-Verwey-Overbeek (DLVO) theory. Addition of salt and thus increase of ionic strength screens the particle charges and consequently should induce attraction. Deviating from this theory, experiments showed that unexpected high ionic strengths are often needed and attraction depends on the nature of the salts (Bénas et al., 2002; Retailleau et al., 2002; Riès-Kautt and Ducruix, 1989). Considering only anions, the increase in attraction follows a direct order of the Hofmeister series (Kunz et al., 2004a) when the protein is studied at a pH above its isoelectric point and the reverse Hofmeister order below the pI.

The salt specificity is still subject of fundamental work (Boström et al., 2004; Kunz et al., 2004b). However, macromolecular interactions in solutions can be characterized by the osmotic second virial coefficient that can be measured by static light scattering (George and Wilson, 1994), small angle x-ray scattering (Finet et al., 2004) or small angle neutron scattering (Velev et al., 1998). Basically, the sign of the second virial coefficient indicates whether the interactions are repulsive or attractive. Slightly negative values in the range of about -1 to $-8 \cdot 10^{-4}\,\mathrm{mol\,ml\,/g^2}$, the so-called "crystallization slot", correlate with conditions that are favorable to crystallization. At more negative values amorphous precipitate is formed preferentially as the protein-protein interactions become stronger and hence, molecules cannot attain their lattice positions and orientations before getting incorporated. At more positive values, the interactions are repulsive and a solid phase is formed only at impractically high protein concentrations.

The change in attraction with increasing salt concentration or other precipitating agents is illustrated by the schematic solubility diagram in fig. 1.

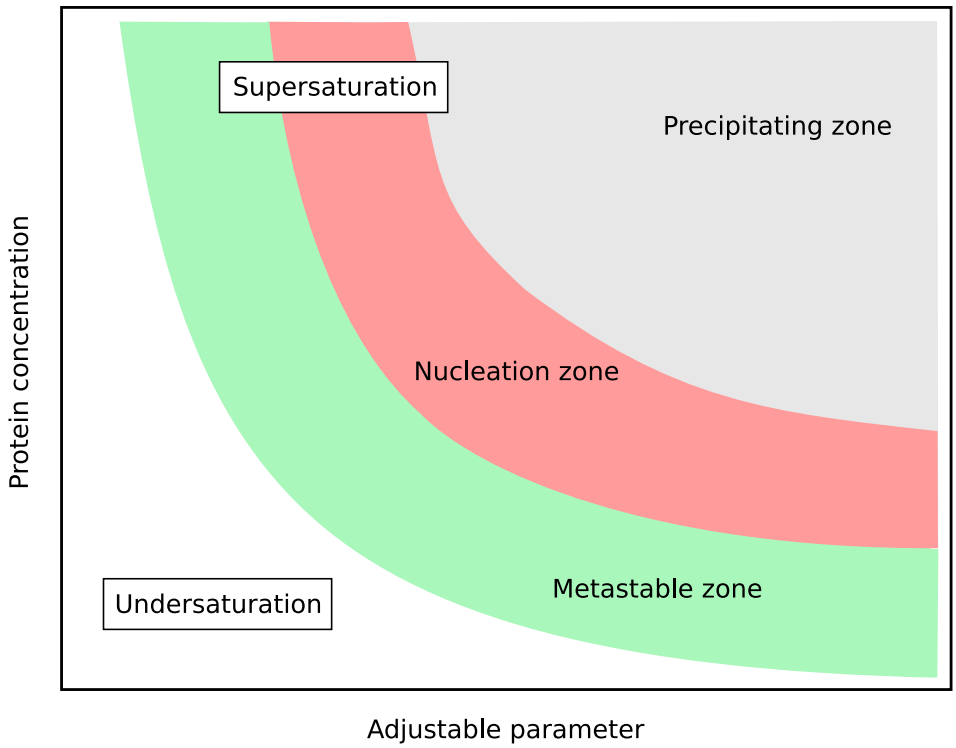

Figure 1: Schematic solubility diagram. The adjustable parameter can be salt or other precipitant concentrations, pH or temperature. In the metastable zone, the supersaturation is low and crystal can grow but has a low probability of nucleation. At intermediate supersaturations, spontaneous nucleation of crystals will take place (nucleation zone). At high supersaturations, the macromolecules will form an amorphous precipitate. The transition between the different zones is not well defined but fuzzy.

In general, crystals are preferentially grown at low supersaturation, which is believed to be beneficial for the quality of crystals if the growth rate is transport controlled. The ensuing decrease in supersaturation at the crystal surface results in a reduction of molecular "landing frequency" that allows molecules with wrong orientation and/or position to detach from the crystal surface and to realign (García-Ruiz, 1999; Vekilov and Chernov, 2002).

1.1.2 Nucleation of protein crystals

A supersaturated solution lowers its free energy by segregating a solid phase. However, spontaneous phase separation is observed only at elevated levels of supersaturation (fig. 1) and small crystallites tend to disappear even in supersaturated solutions in order to eliminate their surface free energies. The reason is the existence of an energy barrier, the so called nucleation barrier, that has to be crossed and the rate limiting step is the formation of a critical nucleus (Oxtoby, 1998).

The topic of nucleation is still controversial, although the main concepts were already developed by Gibbs around 1900 (Gibbs, 1876, 1878, 1993). Most of the nucleation studies have been based on the classical capillary approximation that assumes that nuclei of the new phase have the same molecular arrangements as macroscopic regions of the new phase, i.e. have the same properties (Feher and Kam, 1985; García-Ruiz, 2003). As the new phase is stable, it has a lower free energy than the parent phase. The free energy ΔG_V of a volume occupied by n molecules is given by the difference in chemical potential of molecules in solution μ_P and the solid phase μ_{cryst}.

$$\Delta G_V = -n(\mu_P - \mu_{cryst}) \tag{1}$$

The chemical potentials of the molecules can be expressed as a function of their respective activities by $\mu = \mu^* + RT\ ln\, a$. At equilibrium, the chemical potentials of molecules in solution μ_E and in the solid phase μ_{cryst} are equal and thus, eq. 1 reduces to:

$$\Delta G_V = -n(RT\ \ln a_P - RT\ \ln a_E) = -nRT\ \ln \sigma \tag{2}$$

where σ is the supersaturation; the ratio of the actual activity of molecules in solution and the activity at equilibrium. If the activity coefficients are almost equal to unity, the activities can be replaced by the respective concentrations.

$$\sigma = \frac{a_P}{a_e} \simeq \frac{c_P}{c_e} \tag{3}$$

However, the introduction of a new interface increases the free energy by

$$\Delta G_S = A\,\gamma \tag{4}$$

with A the surface of the new phase and γ the surface free energy per unit area. The surface term is minimized if the nucleus of new phase forms a sphere and hence, this should be the shape of the critical nucleus in most cases. Using v_0, the volume occupied by one molecule in the crystal, and combining eqs. 2 and 4, the total free energy can be expressed as a function of the radius of a spherical nucleus.

$$\Delta G = -\frac{4/3\pi r^3}{v_0} RT\ \ln\sigma + 4\pi r^2\gamma \tag{5}$$

Hence, small nuclei have a positive free energy and tend to dissolve faster than they grow. Upon exceeding a critical size, the nuclei lower their free energy by growing continuously. The interplay of volume and surface contributions to the free energy is illustrated in fig. 2. The critical radius r^*, the nucleation barrier ΔG^* and the number of molecules in the critical nucleus are derived by the condition $d\Delta G/dr = 0$ and are given by

$$r^* = \frac{2v_0\gamma}{k_B T\ \ln\sigma}\ ; \qquad \Delta G^* = \frac{16\pi v_0^2\gamma^3}{3(k_B T\ \ln\sigma)^2}\ ; \qquad n^* = \frac{4/3(r^*)^3}{v_0} \tag{6}$$

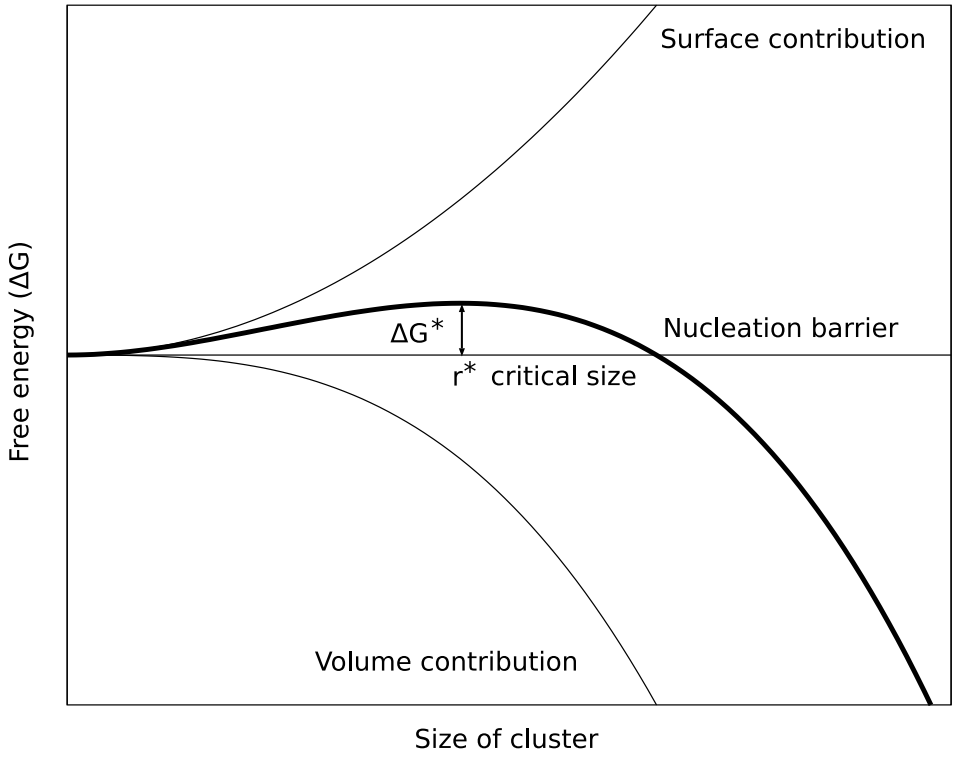

Figure 2: Schematic illustration of the free energy of formation of a spherical cluster according to the classical nucleation theory. Free energy of the cluster is made up of the free energy of the new phase that scales with the volume of the cluster and the surface free energy. ΔG^* and r^* denote the nucleation barrier and the critical size of the cluster, respectively.

Experimentally accessible are the number of crystals grown and the induction time, i.e. the time period prior to the formation of the critical nucleus. The temporal and spatial distributions of density fluctuations occuring in the bulk of the old phase are unpredictable. However, the probability that a density fluctuation reaches critical size is given by $\exp(-\Delta G^*/k_B T)$ according to Boltzmann and the nucleation frequency J, i.e. the number of post-critical

nuclei per unit time and volume, can be expressed as:

$$J = \kappa_0 \exp\left(-\frac{\Delta G^*}{k_B T}\right) = \kappa_0 \exp\left(-\frac{16\pi v_0^2 \gamma^3}{3(k_B T)^3 (\ln \sigma)^2}\right) \tag{7}$$

The corresponding nucleation time for a given volume is usually given by

$$\tau = \tau_0 \exp\left(\frac{\Delta G^*}{k_B T}\right) = \tau_0 \exp\left(\frac{16\pi v_0^2 \gamma^3}{3(k_B T)^3 (\ln \sigma)^2}\right) \tag{8}$$

This is not exactly correct as for $\Delta G^* = 0$, τ should be 0. The coefficients κ and τ_0 are difficult to assess theoretically and are related to the kinetics of attachment of molecules to the nuclei. The experimentally obtained nucleation rates and induction times are random quantities. Hence, to study nucleation it is essential to obtain statistics of the phenomenon by performing multiple nucleation experiments on the same system and under precisely the same conditions.

The exponential increase of the nucleation rate with supersaturation explains the existence of a metastable zone (fig. 1). With decreasing supersaturation the size of the critical nucleus r^* and the nucleation barrier ΔG^* increase and tend to infinity as the supersaturation approaches unity. Consequently, at low supersaturations nucleation of the new phase is not forbidden but very unlikely. With increasing supersaturation, ΔG^* decreases to values comparable to $k_B T$ and lower and the nucleation event becomes probable whereas the nucleation rate increases exponentially.

The limitations of the classical nucleation theory are that the surface free energy of a nucleus is assumed to be equal to that of a crystal interface, the size of critical nucleus decreases smoothly with increasing supersaturation and the

core of a nucleus behaves like the new the new bulk phase, i.e. has crystalline structure. Those assumptions become questionable for nuclei that contain only few tens of molecules. More advanced nucleation theories do account for these problems (Oxtoby, 2003; Oxtoby and Kashchiev, 1994) but nonetheless classical nucleation theory serves fairly well to describe nucleation phenomena.

1.2 Objective

The need for perfect crystals of biological macromolecules is unambiguous (section 1.1). The interest in understanding the different processes involved in crystal growth is reflected by the growing number of participants at the international conferences of crystallization of biological macromolecules (Chernov and DeLucas, 2002).

So far, most studies were focused on the processes of mass transport and incorporation of molecules into the crystals and creation of defects (Chernov, 1997, 2004; García-Ruiz et al., 1999; McPherson, 1999; McPherson et al., 2003; Vekilov and Chernov, 2002; Vekilov and Rosenberger, 1998). Furthermore, the osmotic second virial coefficient was used to identify conditions where crystals grow readily (Bonneté and Vivarès, 2002; Finet et al., 2004; George and Wilson, 1994).

However, much less is known about the processes that are involved in and accompany the birth of crystals. Most information stems from theory (Feher and Kam, 1985; García-Ruiz, 2003; Oxtoby, 1998, 2003; Sear, 2002) and simulation (Lomakin et al., 2003; Tavassoli and Sear, 2002; ten Wolde and Frenkel, 1997). In a few experiments, the critical nucleus itself was subject of investigations. For lysozyme the number of molecules in the critical nucleus was

determined by light microscopy by measuring the nucleation rate (Galkin and Vekilov, 2001) and nuclear magnetic resonance spectroscopy by determining the induction time (Drenth et al., 2003). For apoferritin the critical nucleus was directly observed by atomic force microscopy (Yau and Vekilov, 2000) revealing a quasi-planar shape and for apoferritin, ferritin, pumpkin seed globulin and satellite tobacco mosaic virus the critical size of nuclei was measured by dynamic light scattering (Malkin and McPherson, 1994).

Further, it is still controversial whether the formation of crystallization intermediates between monomers and crystals is a prerequisite for crystal nucleation or not. The formation of aggregates with a fractal structure in supersaturated lysozyme solution was detected by dynamic and static light scattering (Georgalis and Saenger, 1998; Poznanski et al., 2003; Tanaka et al., 1999) and small angle neutron scattering (Niimura et al., 1995). Contrary, independent lysozyme crystallization experiments studied by dynamic light scattering (Muschol and Rosenberger, 1996) and small angle x-ray scattering (Finet et al., 1998) did not find any signs of protein oligomers and hence, could not corroborate these findings.

Up to now, the critical nucleus was only visualized for apoferritin by atomic force microscopy. The observed planar nuclei deviate from the spherical shape predicted by the classical nucleation theory (section 1.1.2) and it is not known whether this shape is common or the planar structure is a particularity of apoferritin.

The aim of this study is to contribute to the unterstanding of structure and identity of aggregates accompanying crystal nucleation. Aggregates and their growth characteristics can be identified by time-resolved dynamic light scattering. Protein clusters, crystal forming or amorphous, shall then be imaged

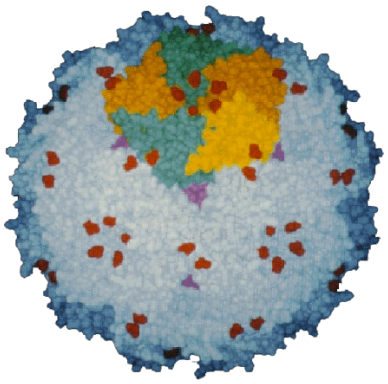

Figure 3: Space filling model of lumazine synthase from *B. subtilis*. 5-fold axes are labeled red, 3-fold axes magenta and two-fold axes red.

by cryo transmission electron microscopy that allows topographical studies at submolecular resolution of protein aggregates while they are still dispersed in solution. For studies of aggregation kinetics along this line, lumazine synthase from *Bacillus subtilis* is an excellent model system due to its size (approx. 16 nm diameter) and reproducible crystallization behavior (section 1.3). For evaluation of the experiments, the solubility and particle interactions of lumazine synthase are needful and consequently, shall be determined too.

1.3 Model system: lumazine synthase from *Bacillus subtilis*

Lumazine synthase from *B. subtilis* is a hollow spherical capside of 60 identical subunits (60 β subunits) arranged in icosahedral symmetry (T=1) with a diameter of 15.7 nm and a total mass of approx. 1 MDa (fig. 3). In complex with the 3 α (riboflavin synthase) subunits, it is involved in the biosynthetic pathway of the vitamin B2, catalyzing the last two steps of riboflavin biosynthesis (Bacher et al., 1980, 1996). In the presence of sodium/potassium phosphate,

pH 8.7, lumazine synthase crystallizes in a hexagonal modification belonging to the space group $P6_322$. The x-ray structure was obtained at 3.3 Å resolution (Ladenstein et al., 1988). Due to its size, symmetry and reproducible crystallization behavior, lumazine synthase was used extensively in our group as model protein to study rotational disorder of protein crystals by electron microscopy (Braun et al., 2000; Tack et al., 1997). In addition, there exists a whole series of lumazine synthases from different hosts that can serve as homologous impurities in crystallization experiments permitting the study of their impact on formation of defects. Lumazine synthase was utilized to study growth of crystals under different solution transport conditions, e.g. diffusion limited growth under microgravity. The influence of changed transport conditions was tested by the quantitative comparsion of point defect densities on crystal surfaces and x-ray diffraction quality (Rodriguez-Fernández, 2003).

2 Results and Discussion

2.1 Solubility of lumazine synthase

Lumazine synthase crystallizes in the presence of sodium/potassium phosphate buffer, pH 8.7, in a hexagonal modification (space group $P6_322$, see Schott et al., 1990 and section 1.3). To determine the equilibrium solubility, several batch crystallization experiments (section 4.2) have been performed at precipitant concentrations ranging from 1.25 to 1.5 M in 0.5 M steps at 20 ℃. The turbidity which was formed immediately upon addition of precipitating agent to the protein solution, disappeared after mixing the solution. Until the first appearance of crystals, the solution remained transparent. Depending on the salt and protein concentration, crystals were observed within hours or days. The conditions and observations for all experiments are summarized in table 1.

Na/K phosphate [M]	c_P [mg/ml]	1st appearance of crystals after	size (longest dimension) and shape of crystals after 1 month
1.25	21	$>$ 14 d	$\geq$ 100 µm, hexagonal plates
1.3	15	4 d	$\approx$ 100 µm, hexagonal plates
1.35	10	5 d	20 – 100 µm, hexagonal plates
1.4	7	1 d	$\approx$ 20 µm, hexagonal plates
1.45	6	overnight	20 + $\geq$ 100 µm, hexagonal plates
1.5	5	$<$ 1 h	30 – 100 µm, hexagonal prisms + hexagonal plates

Table 1: Crystallization of lumazine synthase with an initial protein concentration c_P in sodium/potassium phosphate buffer, pH 8.7 — conditions and observations.

After growth of crystals, the solutions were centrifuged and the supernatant was removed. The crystals were washed twice with the corresponding buffer

	Na/K phosphate, pH 8.7 [M]									
c [M]	0.2	0.9	1.2	1.25	1.3	1.35	1.4	1.45	1.5	1.55
I [M]	0.59	2.66	3.54	3.69	3.84	3.99	4.13	4.28	4.43	4.58
c_E [mg/ml]			7.0	3.9	2.7	1.2	0.55	0.2	0.1	0.05
$\phi_E \cdot 10^4$			84	46.8	33.1	14.7	6.7	2.4	1.2	0.6

Table 2: Solubility of lumazine synthase in mass concentration c_E and volume fraction ϕ_E in different sodium/potassium phosphate buffers, pH 8.7, with concentration c and ionic strength I.

and were allowed to dissolve. After centrifugating the solutions at 15400 rpm, the protein concentration in the supernatant was measured by the Bradford assay (Bradford, 1976). To take into account a possible slow dissolution rate and therefore a slow approach towards the equilibrium state, the concentrations in the supernatant were measured over a period of one month. The steady concentrations after 10 days were taken as solubilities. To determine the solubilities at 1.2 and 1.55 M sodium/potassium phosphate, crystals grown in 1.5 M sodium/potassium phosphate buffer were dissolved in 1.2 and 1.55 M buffers assuming that the crystals grown in different sodium/potassium phosphate buffers have the same modification. However, the salt concentrations within the crystals and the solutions differed. The difference in osmotic pressure can damage the crystals and lead to a dissolution. Thus, the solubilites determined for the 1.2 and 1.55 M sodium/potassium phosphate buffer are less reliable and are presumably too high.

At high phosphate and low protein concentrations, the Bradford assay is less reliable. The phosphate buffer contributes significantly to the measured absorption and samples with protein concentrations lower than 100 µg/ml differ only slightly from the buffer. Table 2 lists all measured solubilities in mass per volume c_E and volume fraction ϕ_E. With increasing salt concentration and

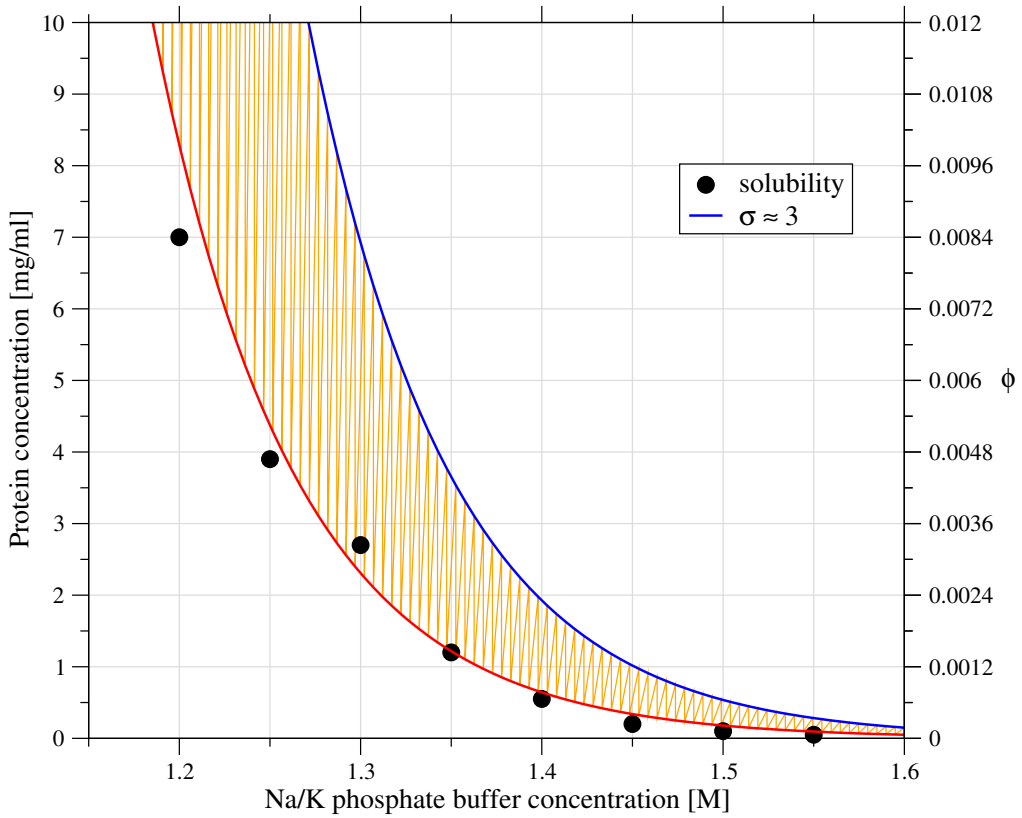

Figure 4: Solubility of lumazine synthase from *B. subtilis* in Na/K phosphate buffer, pH 8.7, in mass concentration and volume fraction ϕ. The blue line corresponds to a supersaturation of 3 ($\sigma = c/c_E$).

thus increasing ionic strength I, the solubility of lumazine synthase decreases.

The protein stock solution contained 0.2 M sodium/potassium phosphate. In earlier sets of crystallization experiments lumazine synthase was stored at a salt concentration of 0.9 M (Braun et al., 2000; Rodriguez-Fernández, 2003). At those salt concentrations and ionic strengths electrostatic repulsions are almost negligible and particle interactions are very short-ranged and attractive (Muschol and Rosenberger, 1995). Comparing the crystallization conditions with those of lysozyme, one would even expect the formation of lumazine

synthase crystals under the storage conditions of $c_P \leq 30$ mg/ml in 0.2 – 0.9 M sodium/potassium phosphate buffer, pH 8.7 (Riès-Kautt and Ducruix, 1989).

Temperature dependence of the solubility of lumazine synthase In search of a temperature dependence of the solubility of lumazine synthase, crystals grown in a broad range of supersaturation and buffer concentration (2–5 mg/ml and 1.3–1.5 M respectively) were exposed to temperature changes. The size of the crystals was monitored in the light microscope to detect differences in solubility. The crystals were grown in batch mode (60 µl, 20 ℃) directly in the pit of an object slide that was covered with a glass slide and sealed with DMS oil. Assuming that crystallization was finished after one month, the object slides were then transferred to the light microscope that was equipped with a temperature controlled stage that was especially built for these crystallization experiments (section 4.4.1). The samples were cooled down from 20 ℃ to 8 ℃ or heated up to 32 ℃ within 30 minutes and stored at the final temperature for 8 hours. No change in size and shape of the crystals could be detected for any sample. Thus, it was concluded that the solubility of lumazine synthase is almost independent of temperature at least in the investigated range.

This result is not totally unexpected. The phase diagram calculated for particles with short-range interactions shows a very small change of solubility with temperature at low protein concentrations (shown in fig. 5, Rosenbaum and Zukoski, 1996; Vliegenthart and Lekkerker, 2000). A change in solubility with temperature can be expected for solubilities at higher volume fractions corresponding to crystallization at lower salt concentrations (Guilloteau et al., 1992). For example, lysozyme shows almost no temperature dependence in

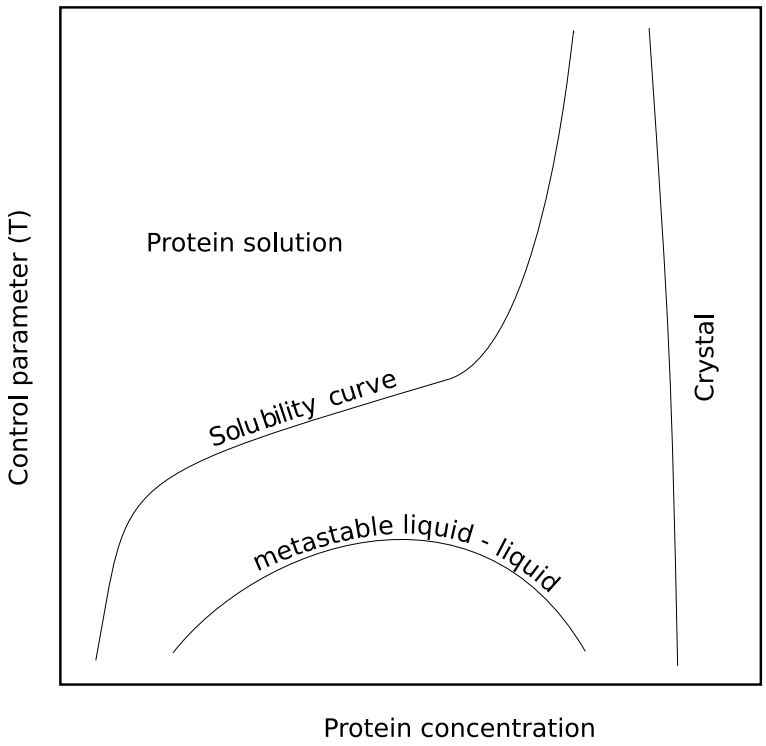

Figure 5: Schematic phase diagram of protein solutions with short-range attractive interactions.

the range from 10 ℃ to 30 ℃ at a salt concentration of 7 % (w/v) sodium chloride whereas at 3 % (w/v) sodium chloride the solubility changes significantly with an even more pronounced effect at higher temperatures (Muschol and Rosenberger, 1997).

2.2 Particle interactions of lumazine synthase

2.2.1 2nd virial coefficient

The solubility of lumazine synthase decreases about two magnitudes when the salt concentration is increased from 1.25 to 1.55 M (25 %). This decrease in solubility is equivalent to a decrease in repulsive interactions and crystallization occurs in attractive regimes or nearby (Ducruix et al., 1996; George and Wilson, 1994; Muschol and Rosenberger, 1995; Velev et al., 1998; Yau et al., 2000). To characterize the particle interactions, the osmotic second virial coefficient A_2 was measured by static light scattering using the relationship between the Rayleigh ratio R_θ and the mass concentration of the protein c_P (section 4.3.1; Schmitz, 1990; Zimm, 1948):

$$\frac{K \cdot c_P}{R_\theta} = \frac{1}{M_P} + 2A_2 \cdot c_P \tag{9}$$

with

$$K = \frac{4\pi^2 n_\circ^2 (\frac{dn}{dc})^2}{N_A \lambda^4} \tag{10}$$

In eqs. 9 and 10, M_P is the molar weight of the protein, N_A Avogadro's number, $n_\circ$ the refractive index of the buffer solution, λ the wavelength of the scattered light, θ the scattering angle and dn/dc the refractive index increment.

As the used refractive index detector operates with white light and not at the correct wavelength of 690 nm, the measured dn/dc of 0.21 ml/g contains an error (section 4.3.1). For aqueous systems, this difference is about 5 % (Roessner, 1996) and thus the correct molar mass and 2nd virial coefficients should be 10 % smaller and larger, respectively. The scattering intensity data for the various salt concentrations extrapolated to zero angle are presented in fig. 6

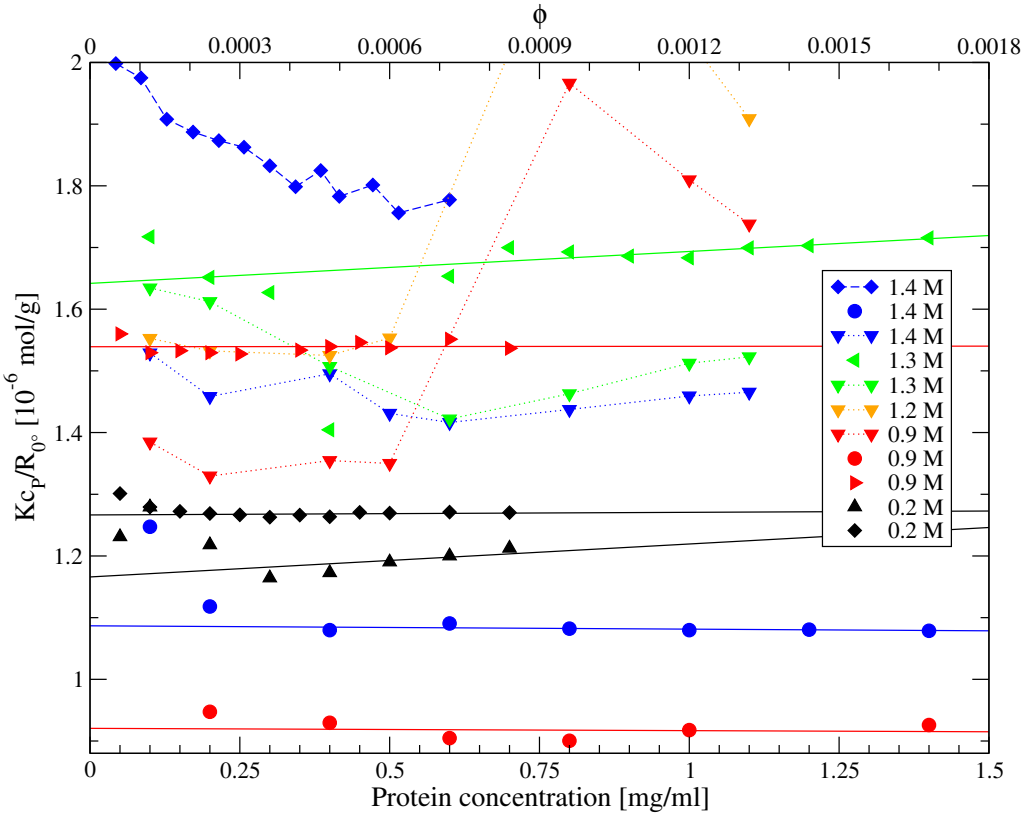

Figure 6: Debye plots for lumazine synthase solutions in sodium/potassium phosphate buffer, pH 8.7. Same salt concentrations have the same color: 0.2 M black, 0.9 M red, 1.2 M orange, 1.3 M green, 1.4 M blue. The results of the least squares fits to eq. 9 (solid lines) are listed in table 3.

as Debye-plots of the scattering ratio Kc_P/R_{0° versus protein concentration c_P and corresponding volume fraction ϕ. The results of the least square fits to eq. 9 are presented in table 3 and fig. 7. The intercepts at $c_P = 0$ yield the molecular weight and the 2nd virial coefficient A_2 is obtained from the slope of the fitted lines. The experiments exhibiting a discontinuous curve progression (dotted lines in fig. 6) were excluded from further analysis.

Fig. 6 reveals three main features: the calculated molar masses vary drastically, in most of the cases being smaller than the published value ($M_P \approx$

c_{salt} [M]	M [10^3 g/mol]	A_2 [10^{-6} mol · ml/g^2]	B_2
0.2	858	26.7	0.59
0.2	790	2.1	$4.6 \cdot 10^{-2}$
0.9	650	0.3	$6.6 \cdot 10^{-3}$
0.9	1086	- 1.8	$-4.0 \cdot 10^{-2}$
1.3	609	25.8	0.57
1.4	920	- 2.7	$-5.9 \cdot 10^{-2}$

Table 3: Calculated molar mass and 2nd virial coefficients of lumazine synthase in sodium/potassium phosphate buffer, pH 8.7.

1 MDa; Schott et al., 1990) and the slope of Kc_P/R_{0° with c_P and thus the 2nd virial coefficient is almost zero for all examined conditions.

In the following, the variance of the molar mass and its deviation from the true value shall be discussed. Among the variables contributing to eq. 9 the protein concentration and the refractive index increment show the largest inaccuracy. The protein concentration is determined by the Bradford assay. This method has an error of ±10 %. In addition, the samples were filtered prior to the light scattering experiment (section 4.3.1). Thus, a limited amount of protein was removed from the samples. As mentioned above, the refractive index increment was determined with limited confidence. In addition, the refractive index increment of a protein solution depends not only on the protein, but also on the type and the concentration of the solvent (Ball and Ramsden, 1998; Fasman, 1976; Yin et al., 2003).

In fig. 6, Kc_P/R_{0° increases at low concentrations and deviates from the linear slope for all experiments. This is attributed to a decrease in protein concentration due to the filtering prior to light scattering experiments. The error introduced is more aggravating at low concentrations and results in smaller determined molar masses and “more negative” 2nd virial coefficients. Hence,

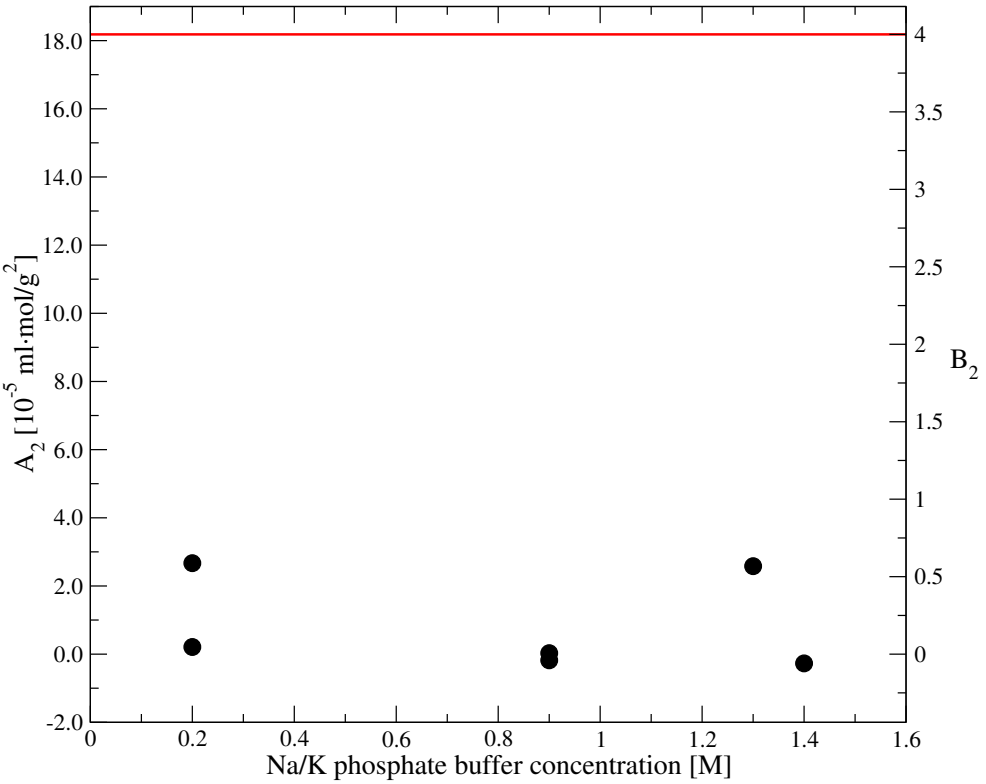

Figure 7: 2nd virial coefficients (in $\mathrm{mol} \cdot \mathrm{ml/g^2}$ and dimensionless) of lumazine synthase for different sodium/potassium phosphate phosphate concentrations, pH 8.7. Red line shows the 2nd virial coefficient for "hard spheres" ($B_2 = 4$).

the data points for the lowest protein concentrations (0.05 up to 0.15 mg/ml) were not included in the regression analysis.

A relative error in protein concentration changes the molar mass linearly whereas a difference in the refractive index increment contributes as quadratic term to the molar mass and the second virial coefficient. For example, using values that are 10 % too high for both the protein concentration and the refractive index increment, the calculated molar mass decreases by 33 % whereas the 2nd virial coefficient increases by 21 %.

Considering these inaccuracies, the calculated masses coincide fairly well

with the predicted one assuming that the refractive index increment at λ = 690 nm is lower by 10 % ($dn/dc \approx 0.19$ ml/g). Three experiments do not fit this picture; the topmost (blue, dashed line, 1.4 M) and the two lowest datasets in fig. 6 (blue 1.4 M and red 0.9 M). The deviation of the first one cannot be explained with the above mentioned arguments. Thus, its results are not discussed further. The other two experiments show an angular dependence in their scattering intensity contrary to all other experiments (not shown). This indicates partly aggregated samples. Consistently, the calculated molar masses are higher than for the other experiments. Both samples were prepared from the same stock solution. Thus, the difference in mass cannot be attributed to concentration differences alone. Interestingly, the sample with lower salt concentration (0.9 M) shows "stronger aggregation" (higher molar mass). Normally the opposite is expected. At a salt concentration of 1.4 M sodium/potassium phosphate the solubility of lumazine synthase is 0.55 mg/ml whereas at 0.9 M the protein can be stored at concentrations higher than 30 mg/ml (table 2 and fig.4). Thus, it is eligible to assume that the particle interaction is more attractive at the higher salt concentration. The aggregates should grow and the calculated molecular weight should be larger. By filtering the solutions, most of the aggregates in the 1.4 M solution were removed. The mean molar mass is still larger than in most other experiments but smaller than for the experiment at 0.9 M. The reduction in protein concentration is very small as most of the protein is present as single molecules (section 2.3). In addition, the lower mass found at 1.4 M salt concentration can be explained to a minor degree by a dependence of the refractive index increment on the salt concentration as well. A decrease in dn/dc results in larger molar masses. This assumption is supported by the relative high molecular weight found for

the experiments conducted at 0.2 M sodium/potassium phosphate. This implies that at increased salt concentrations the 2nd virial coefficients are even smaller.

George and Wilson made the observation that osmotic 2nd virial coefficients for proteins near crystallization fall within a narrow range of slightly negative values from about -1 to $-8 \cdot 10^{-4}$ mol ml /g^2, the so-called "crystallization slot" (George and Wilson, 1994). More recently, the solubility could be correlated with the 2nd virial coefficient (Guo et al., 1999; Haas et al., 1999).

The 2nd osmotic virial coefficient of lumazine synthase was determined in a broad range of salt concentrations corresponding to more repulsive conditions, where the protein can be stored for months (0.2 and 0.9 M sodium/potassium phosphate, $c_E > 30$ mg/ml), and more attractive conditions, where the protein crystallizes readily (1.3 and 1.4 M, $c_E < 3$ mg/ml). Contrary to the observed change in solubility, the determined virial coefficients are very small, almost 0. A_2 ranges from $-3 \cdot 10^{-6}$ to $3 \cdot 10^{-5}$ mol ml/g^2. Considering the preceding error discussion, the absolute values should even be smaller with a more profound effect at higher salt concentrations. Thus, crystallization of lumazine synthase occurs at conditions where it is not predicted by the "crystallization slot". More aggravating is that the stock solution is stored at the same apparent "interaction conditions" as the crystallizing solutions.

2.2.2 Particle pair interaction potential

To explain the above contradiction, the relation between the osmotic 2nd virial coefficient and the particle interaction has to be addressed in more detail. Regardless of the kind of scattered radiation, the intensity scattered by particles

in solution is the product of three contributions (Georgalis and Saenger, 1998; Luzzati and Tardieu, 1980; Piazza, 2000):

$$R_\theta = K\, M_P\, c_P\, P(q)\, S(q, c_P) \tag{11}$$

a "contrast term" summing up the specific interaction between the sample and the given radiation (for light K and the refractive indices), the "form factor" $P(q)$, which depends on the particle geometry and the "structure factor" $S(q, c_P)$ which accounts for inter-particle effects. q^{-1} is the length scale over which the solution is probed, where q is the length of the wave vector defined as $q = (4\pi n_0/\lambda) \cdot sin(\theta/2)$. For particles much smaller than the wavelength of the scattering light the form factor is almost equal to 1 ($P(q) \approx 1$) over the range of accessible wave vectors q. Combining eqs. 9 and 11 the structure factor is in the zero-q limit:

$$\frac{1}{S(0, c_P)} = 1 + 2\, M_P\, A_2\, c_P \quad \text{or} \quad S(0, c_P) \approx 1 - 2\, M_P\, A_2\, c_P \tag{12}$$

The $S(q, c_P)$ itself is related to the pair interaction potential $U(r)$ through the radial distribution function $g(r)$, which is basically the probability of finding two particles at a mutual distance r (Chandler, 1987; McQuarrie, 2000):

$$S(q, c_P) = 1 + \rho_n \int (g(r) - 1) \mathrm{e}^{i\mathbf{q}\cdot\mathbf{r}} d\mathbf{r} \tag{13}$$

where $\rho_n = c_P\, N_A/M_P$ is the number density of particles. In the low density limit, where the potential energy of the system is pair-wise additive, $g(r)$ can be approximated by $exp(-U(r)/k_B T)$, with $k_B T$ the thermal energy. Thus

the 2nd virial coefficient can be expressed as:

$$A_2 = \frac{N_A\, 2\pi}{M_P^2} \int_0^\infty \left(1 - \mathrm{e}^{\frac{-U(r)}{k_B T}}\right) r^2\, dr \tag{14}$$

or by defining a dimensionless 2nd virial coefficient $B_2 = M_P^2\, A_2 / V_P\, N_A = M_P^2\, A_2 / (4/3\pi a^3\, N_A)$, with V_P and a the volume and radius of the particle (Bonneté and Vivarès, 2002; Petsev and Vekilov, 2000; Vliegenthart and Lekkerker, 2000):

$$B_2 = \frac{3}{4\, a^3} \int_0^\infty \left(1 - \mathrm{e}^{\frac{-U(r)}{k_B T}}\right) r^2\, dr \tag{15}$$

To summarize, the 2nd virial coefficient is a function of the pair interaction potential. However, as it is only a summation of all structural features in a single number, it is a quite indirect characterization of particle interactions that can only show that the experimental results are consistent with a chosen potential.

For instance, for spherical particles interacting only through excluded volume repulsion, "hard sphere potential", the dimensionless 2nd virial coefficient solves to $B_2^{HS} = 4$ ($U(r) = \infty$ for $r < a$ and $U(r) = 0$ for $r > a$). Values below 4 signalize attractive interactions compared to the hard sphere potential that can lead to crystallization. Remember that hard spheres do form readily a fcc phase at particle volume fractions of 0.5 due to entropic effects only.

Bonneté and Vliegenhart recalculated A_2 for various proteins in terms of $B_2 = M_P^2\, A_2 / V_e\, N_A$ and $B_2 = A_2\, M_P\, d$ respectively, being V_e and d the excluded volume and the average mass density of proteins ($d = 1.36\ g/cm^3$), resepectively (Bonneté and Vivarès, 2002; Vliegenthart and Lekkerker, 2000). For almost all proteins examined, the optimum crystallization conditions cor-

respond to B_2 values varying between -4 and -40. The only protein which did not fit this picture and crystallizes at a similar virial coefficient as lumazine synthase was Brome mosaic virus (BMV) (Casselyn et al., 2001). BMV is a large macromolecule ($a = 13.4\,\mathrm{nm}$, $M_P \approx 4.6\,\mathrm{MDa}$) that crystallizes in the presence of PEG 8000 ($> 6\,\%\,(\mathrm{w/v})$) with $B_2 < 3$. Apoferritin is also known to crystallize in the presence of cadmium ions at the low end of the crystallization slot ($-3 < B_2 < 0.4$; Petsev et al., 2001). Thus, it seems that positive values of the 2nd virial coefficient are compatible with the formation of crystals as long as they are smaller than B_2^{HS}.

It remains controversial why the second virial coefficient does not decrease with increasing salt concentration. B_2 of lumazine synthase is always smaller than 4 and thus compared to a system of hard spheres the interactions should be attractive. The reason why no crystals are observed at relative low salt concentrations could be that the protein concentration is not elevated enough. Addition of sodium/potassium phosphate lowers the solubility due to a subtle change in the pair interaction potential that is too small to be resolved in terms of the 2nd virial coefficient because of limitations of the measurements (section 2.2.1). This explanation alone is questionable. Usually, the change in B_2 accompanying the decrease in solubility as observed for lumazine synthase upon addition of precipitating agent is at least 4 time larger than the total range of B_2 values found for this system (table 3; Finet et al., 2004).

More likely is a counterbalanced interplay of attractive and repulsive forces. The 2nd virial coefficient is essentially an integration of the pair interaction potential over all distances weighted with the square of the distance (eq. 15). Hence, small changes of the potential curvature can have an emphasized effect on the second virial coefficient. As a consequence, following picture can be

envisioned: Due to the salting out effect (Edwards and Williams, 2004; Kunz et al., 2004a) solubility decreases along with an increase of attractive interactions at short length scales. Thus, the pair interaction potential becomes more negative in the direct vicinity of the particle. Due to solvent structuring (Israelachvili and Wennerström, 1996; Netz, 2004; Svergun et al., 1998) a long-range repulsive interaction contributes to the potential. The formation of an adsorption shell of hydrated sodium ions around the protein at elevated buffer concentrations has been suggested for apoferritin (Paunov et al., 2001; Petsev and Vekilov, 2000).

Those explanations are somehow speculative and cannot be confirmed or excluded by the 2nd virial coefficient alone. The exact knowledge of the energy landscape is necessary to answer these open questions. The pair interaction potential and the pair distribution function are directly accessible through the structure factor. With static light scattering the structure factor can be determined only in the low-q limit whereas neutron or X-ray scattering allows the measurement of $S(q)$ over a wide q-range due to their small wavelength (Luzzati and Tardieu, 1980; Niimura et al., 1995). Especially neutron scattering is valuable because of the different contrast of protein and hydration shell (Svergun et al., 1998).

2.3 Nucleation of lumazine synthase crystals

To characterize the earliest stages of crystallization of lumazine synthase, supersaturated solutions were studied by time resolved dynamic light scattering and cryo transmission electron microscopy (sections 4.3.2 and 4.4.2). The solutions contained varying concentrations of lumazine synthase (1 to 16 mg/ml) and sodium/potassium phosphate (0.2 to 1.5 M, pH 8.7).

2.3.1 Dynamic light scattering

In undersaturated solutions of lumazine synthase containing 0.2 M sodium/ potassium phosphate, pH 8.7, only single molecules were found by dynamic light scattering. The calculated hydrodynamic radius of $R_h = 8$ nm coincides well with the radius of 7.85 nm determined by x-ray crystallographic analysis (Ladenstein et al., 1988). In the range of investigated protein concentrations from $c_P = 1$ to 16 mg/ml, no dependence of the size on protein concentration was found. The particle size distributions were relative monodisperse with a relative variance of less than 0.12. The relative variance is defined as standard deviation of the particle distribution divided by the mean radius. Less than 1 % of all recorded spectra exhibited the presence of larger species (> 500 nm) that were attributed to air bubbles or dust.

In order to investigate the aggregation phenomena occurring in supersaturated solutions of lumazine synthase, conditions that were compatible with the time scale of dynamic light scattering measurements had to be identified. Aggregation kinetics have to be slow enough, that the particle size distribution can be assumed to stay constant within a single measurement (30 s, section 4.3.2). On the other hand, nucleation has to be frequent enough to be

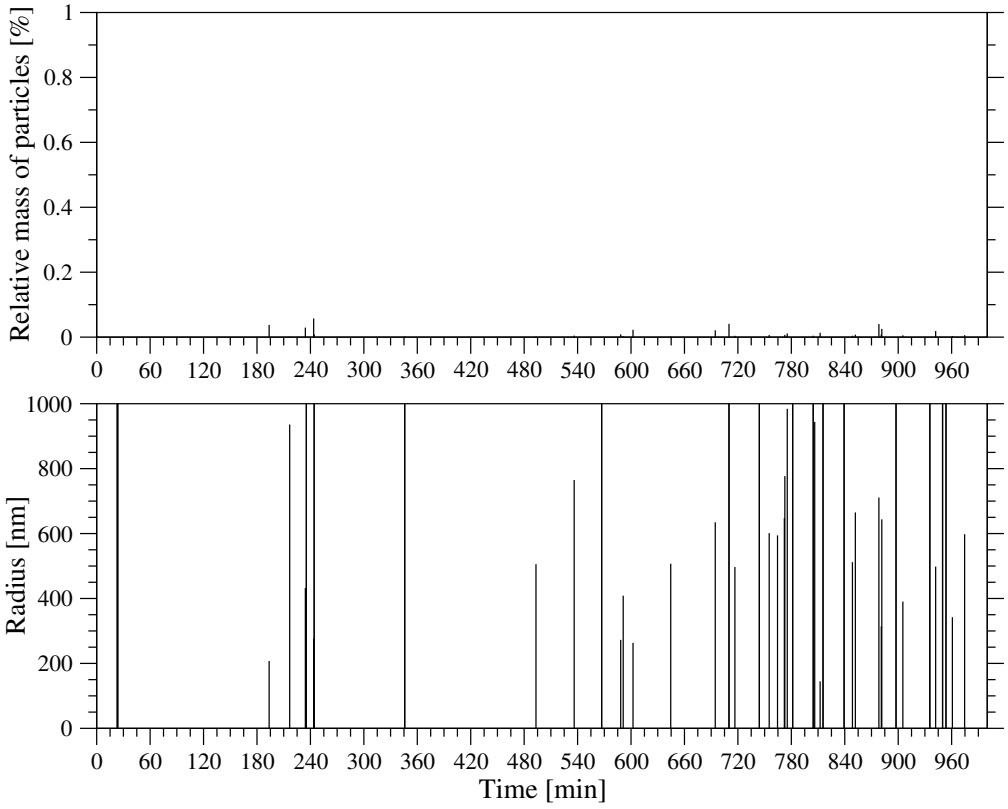

Figure 8: Time-resolved DLS: Time evolution of the average sizes and relative masses of aggregates of lumazine synthase at c_P = 3 mg/ml in 1.5 M sodium/potassium phosphate buffer, pH 8.7. Monomers are not shown (R_h = 8 nm).

observed.

When the protein concentration is increased from 3 to 5 mg/ml at a constant salt concentration of 1.5 M sodium/potassium phosphate, pH 8.7, the moment of first appearance of crystals shifts from a day to less than an hour. Fig. 8 shows the time evolution of the average sizes and relative masses of aggregates of lumazine synthase at c_P = 3 mg/ml. Autocorrelation functions were recorded directly after mixing the solutions. Most spectra showed only the presence of the single lumazine synthase molecules, with a hydrodynamic

radius of 8 nm (not shown in fig. 8). A minor fraction of all measurements revealed a second population with a broad size distribution (variance > 0.3) and its mean radius ranging from 100 nm to more than a micrometer with a total weight of less than 0.1 % in mass (fig. 8). In less than 1 % of all collected datasets the autocorrelation functions were best fitted by the sums of 3 or more exponential decays. As no more than 2 populations can be identified simultaneously with confidence by dynamic light scattering, these datasets were ignored. The frequency of observation of larger particles increased with time. In the particular experiment shown in fig. 8, 3 % of all records revealed larger particles within the first 8 to 9 hours. After this period of time, the frequency increased to 12 % and remained constant until the recording of spectra was stopped after 22 hours (not shown). At the end of the experiment, i.e. after 22 hours, the solution was examined under the light microscope. Only very few crystals with a diameter of about 150 µm were observed and the protein concentration remained almost unchanged as estimated from the total scattering intensity of the sample.

Numerous crystallization experiments were performed in 1.4, 1.45 and 1.5 M sodium/potassium phosphate buffer, pH 8.7, showing similar aggregation pattern. To summarize, two regimes could be distinguished. At the beginning of all crystallization experiments, the probability for detection of larger particles was low. With time, the frequency increased whereas the onset depended on supersaturation. The mass fraction of lumazine synthase of less than 0.1 % contained in the aggregates was still very low. The exact moment of onset of growth of aggregates could not be determined as no continuous growth in size and mass was observed. In addition, crystallization experiments at virtually unchanged conditions always differed in their aggregation behavior, i.e. in the

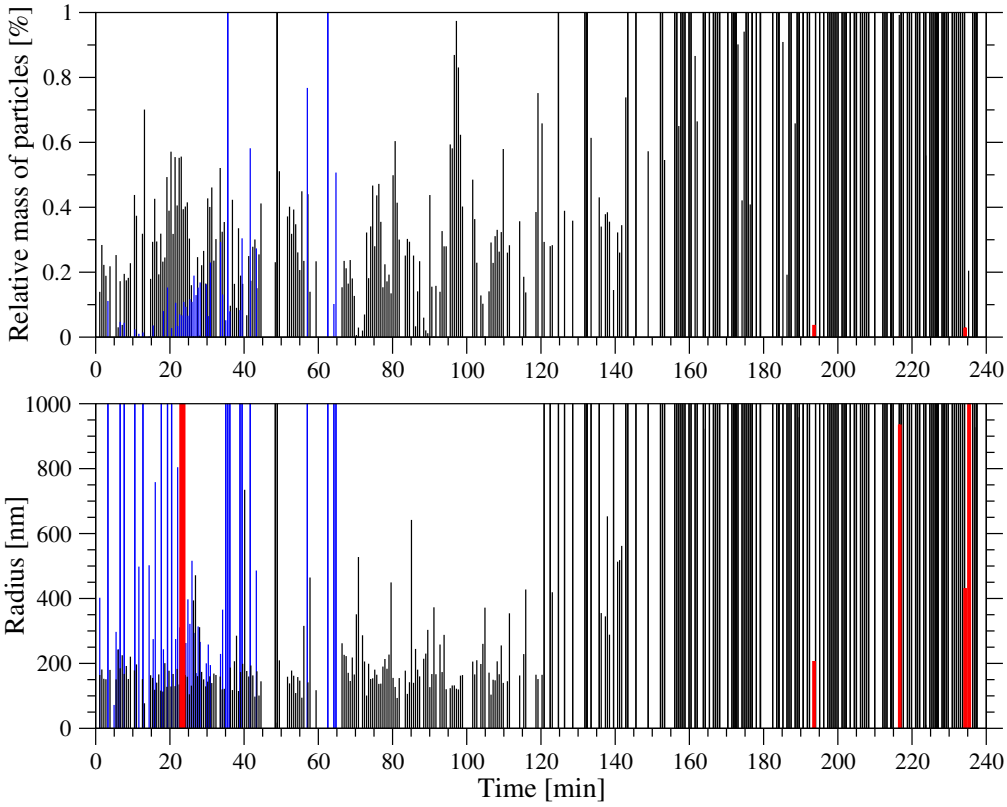

Figure 9: Time-resolved DLS: Time evolution of the average sizes and relative masses of aggregates of lumazine synthase in 1.5 M sodium/potassium phosphate buffer, pH 8.7. Black and blue bars: two different experiments at c_P = 3.5 mg/ml. Red bars: c_P = 3 mg/ml, same experiment as in figure 8. Monomers are not shown (R_h = 8 nm).

onset of increased detection of aggregates. Thus, the induction period prior to growth of aggregates could not be determined and could not be correlated with the supersaturation to calculate the critical size of the nucleus.

At higher supersaturations, the first stage vanished almost completely. Fig. 9 shows the time evolution of aggregates at c_P = 3.5 mg/ml for two different experiments in 1.5 M sodium/potassium phosphate buffer, pH 8.7 (black and blue bars). For comparison the data from the experiment at c_P = 3 mg/ml

(fig. 8) are included as well (red bars). At c_P =3.5 mg/ml, aggregates were present almost from the beginning on (black bars). The sizes were more defined with a hydrodynamic radius of $R_h \simeq 150$ nm and the aggregates were more abundant with a relative mass of 0.2 %. Fig. 9 shows areas where no aggregates are present, for instance from t = 45 to 47 minutes, which correspond to regions, where more than two populations were detected and thus the datasets were ignored or where samples were taken for electron microscopic examination (t = 0 min, 10 min, 33 min, 61 min). After 2 hours, total mass of aggregates increased significantly up to 3 %. The spectra were dominated by larger aggregates, presumably microcrystals, and in about 2 % of all recorded autocorrelation functions from t = 120 to 240 minutes lumazine synthase molecules were no longer detected. The calculated sizes of aggregates ranged from tens of nanometers to several micrometers. The number of scatterers contributing to the autocorrelation functions changed considerably (number fluctuation) and the computed particle size distributions were flawed. During the course of further data acquisition the autocorrelation functions became so erroneous that they were best fitted by the sums of three or more exponential decays.

Taking samples to the light microscope at t = 1 h, appearance and growth of crystals from a clear solution was observed waiting a few minutes. Apparently the particles that dominate the spectra were too small to be observed in the light microscope but did grow easily to visible dimensions.

A different experiment at virtually the same conditions (blue bars in fig. 9) showed faster aggregation. In the first ten minutes, the calculated size distributions were still broad ranging from 100 nm to several micrometers in radius and the relative mass was very low with a mass fraction of less than 0.1 %.

With time, the relative mass of aggregates increased to 0.2 %, the calculated radii varied less and increased from about 200 to 300 nm (t > 18 min). After 40 minutes, the spectra were governed by number fluctuations and all further datasets were discarded. In both experiments crystallization was almost finished after two days with crystal sizes ranging from 10 to 30 µm. The reason for the different aggregation behavior of lumazine synthase observed in the two experiments can be attributed to a slightly higher supersaturation in the second experiment or to a small variance in mixing the samples causing different local supersaturations for a short moment.

At c_P = 4 mg/ml, the autocorrelation functions were impaired by number fluctuations and did not decay to zero almost immediately after mixing the protein solution and precipitating agent and starting data acquisition. 6 hours later, crystals and needle-like structures were observed under the light microscope (fig. 10). The latter disappeared within one day in favor of the crystals. These needle-like structures were observed in earlier crystallization experiments performed in our group in 1.55 M sodium/potassium phosphate buffer, pH 8.7, at c_P = 10 mg/ml and in 1.6 M buffer at a temperature of 10 °C with c_P = 8 mg/ml. The needles have a thickness of approximately 60 nm and grow to lengths ranging from 280 nm to several micrometers. Within the needles, lumazine synthase molecules were observed to be orthogonally packed whereas no rotational order could be found (Rodriguez-Fernández, 2003; Tack, 1997).

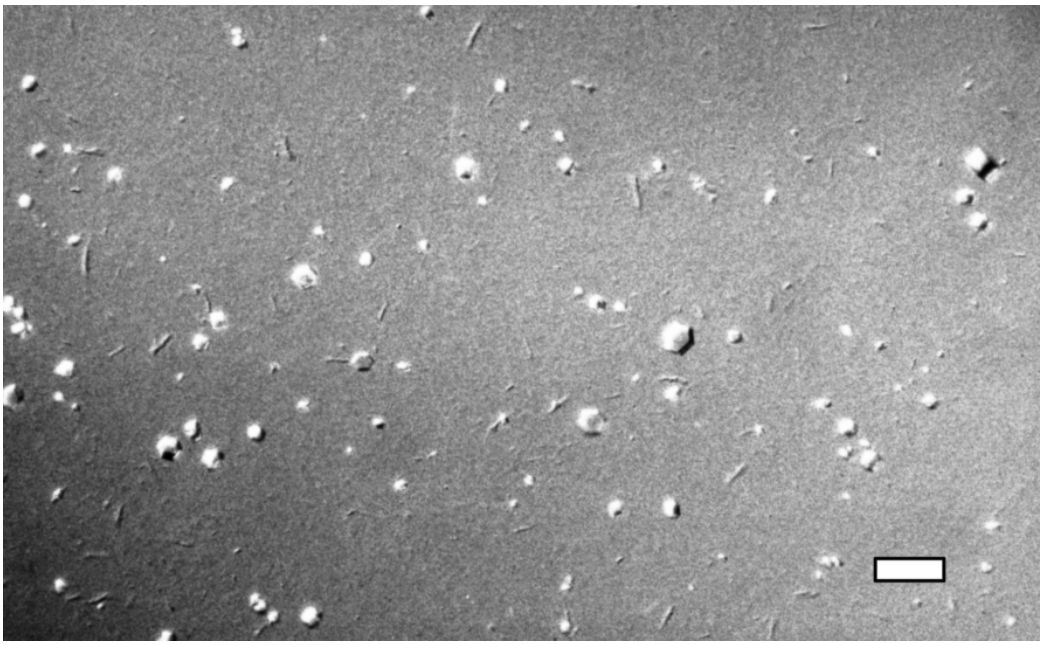

Figure 10: Light micrograph of a crystallizing lumazine synthase solution (c_P = 4 mg/ml, 1.5 M sodium/potassium phosphate buffer, pH 8.7) 6 hours after mixing the protein and the precipitant solutions (scale bar = 100 µm).

2.3.2 Cryo transmission electron microscopy

The critical nucleus is in a transition state and as such energetically unfavored. Consequently, the concentration of this particle should be negligible. Near-critical nuclei, clusters with dimensions smaller or larger than the critical nucleus are more stable and therefore have a longer lifetime. Thus, it should be possible to directly observe those clusters by imaging methods. In 1.5 M sodium/potassium phosphate buffer, pH 8.7, nucleation rate of crystals is increased significantly at lumazine synthase concentrations above 3 mg/ml and consequently, the probability to observe near-critical nuclei is enhanced.

To image the clusters linked to crystal growth and the critical nucleus, supersaturated lumazine synthase solutions were analyzed by cryo transmission

electron microscopy. Samples were taken directly out of the light scattering cuvette and prepared as described in section 4.4.2. This procedure allowed to correlate particle size distributions derived by dynamic light scattering with the structures visualized by electron microscopy.

Cryo samples were taken from the crystallization experiments at protein concentrations of 3 mg/ml and 3.5 mg/ml in 1.5 M sodium/potassium phosphate buffer, pH 8.7, presented before (fig. 8 and fig. 9, black bars) at t = 0 min, 3 min, 7 min, 17 min, 27 min, 42 min and t = 0 min, 10 min, 33 min, 61 min, respectively. Only in the samples taken at t = 27 min and 42 min from the 3 mg/ml lumazine synthase solution and the sample taken directly after preparing the 3.5 mg/ml solution, lumazine synthase molecules could be identified. In all other cryo-samples either the ice-layer was too thick because of insufficient blotting or sample contamination or samples were blotted too long and the holes were empty or the holey carbon film was detached from the carbon grid.

Figs. 11A and 11B show cryo-TEM micrographs taken from the 3 mg/ml and the 3.5 mg/ml lumazine synthase solutions 27 min and directly after starting the crystallization experiments, respectively. Molecules are difficult to identify as the contrast stems from the relative low density difference between protein (1.36 g/cm^3) and solvent (1.20 g/cm^3, table 6 in section 4.3.2) and the difference in scattering cross section of the atoms in the lumazine synthase molecules and the sodium/potassium phosphate buffer whereas the scattering cross section increases with $Z^{3/2}$, with Z the atomic number.

Both micrographs show crowded solutions. Fig 11A shows a network of lumazine synthase aggregates. However, it is difficult to discern whether the molecules and aggregates are interconnected or not. In the higher supersat-

urated solution also clusters with a linear arrangement of the molecules are observed, consisting of 5 to 10 single particles (fig. 11B, red line).

The sizes of the aggregates determined by dynamic light scattering and electron microscopy roughly match. At lower supersaturation, the size distribution of aggregates varied over a broad range from hundreds of nanometeters to a few micrometers. This can be explained by the structures seen in fig. 11A. If the aggregates move independently, smaller radii are detected by dynamic light scattering. Upon agglomeration, they move together as a large body through the solution and thus the detected size becomes larger. In the experiment at c_P = 3.5 mg/ml, the clusters seen with the electron microscope are smaller than predicted by dynamic light scattering. The longest dimension of the linear aggregates is only as large as the mean radius of the aggregates of about 150 nm determined by dynamic light scattering.

Another contradiction is that light scattering experiments indicate that aggregates should have been less frequently observed than single lumazine synthase molecules as the relative mass of aggregates was less than 1 % (Figs. 8 and 9). However, the electron micrographs exhibit almost only aggregates. Counting the number of lumazine synthase molecules on electron micrographs of frozen solution of 0.2 M sodium/potassium phosphate buffer with c_P = 5 mg/ml, in squares of 200 nm × 200 nm and assuming the thickness of the frozen solution as 300 nm, the calculated protein concentration in the examined ice layers is at least 4 times too high. In addition, the solvent has a higher contrast than the lumazine synthase molecules as the solvent is darker than the proteins on the electron micrographs. But the protein is slightly denser than the solvent in 1.5 M sodium/potassium phosphate buffer and the protein should appear darker. All these observations together suggest that the sol-

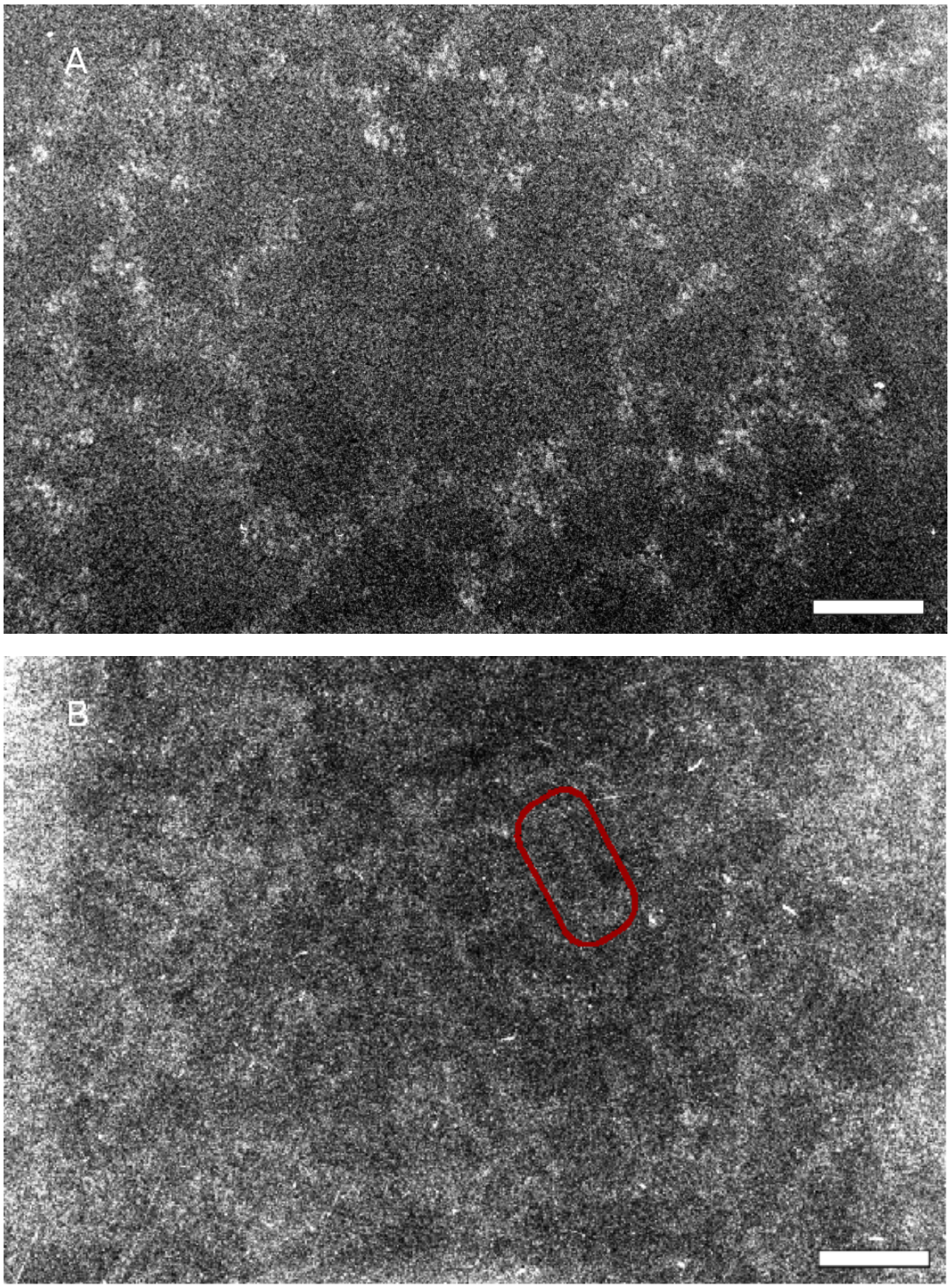

Figure 11: Cryo-transmission electron micrographs of crystallizing lumazine synthase in 1.5 M sodium/potassium phosphate buffer, pH 8.7 (scale bar = 100 nm). A) c_P = 3 mg/ml, sample taken 27 minutes after mixing solutions, same experiment as presented in fig. 8. B) c_P = 3.5 mg/ml, sample taken directly after mixing solutions, same experiment as presented in fig. 9 (black bars).

vent evaporated during sample preparation, presumably between blotting and freezing of the sample. Therefore, it cannot be ruled out that the aggregates seen with the electron microscope are artefacts of sample preparation.

2.3.3 Discussion

Dynamic light scattering has already been used successfully to estimate the size of critical nucleus of supersaturated solutions of pumpkin seed globulin, apoferritin and satellite tobacco mosaic virus (Malkin et al., 1993; Malkin and McPherson, 1993a,b). Continuous aggregation leading to the formation of crystals was established after an induction period and the size of critical nucleus was estimated as greatest average size of aggregates within this induction period. Crystals were observed within 1 and 5 days at relative moderate supersaturations and the size of critical nucleus was found to be $R_h \sim 22$ nm and 32 nm at $\sigma = 1.3$ and 1.2 for pumpkin seed globulin ($R_h = 2.9$ nm) and $R_h \sim 20$ nm and 26 nm at $\sigma = 2.5$ and 2.1 for apoferritin ($R_h = 6$ nm), respectively.

In solutions of lumazine synthase at similar supersaturations ($c_P \sim 1$ mg/ml at $\sigma = 10$ in 1.5 M sodium/potassium phosphate buffer, pH 8.7 and $c_P \sim 1$ mg/ml at $\sigma = 2$ in 1.4 M sodium/potassium phosphate buffer, pH 8.7) almost no aggregates were detected. Particle size distributions were similar to those presented in fig. 8 during the first hours. At higher supersaturations, e.g. at $\sigma \gg 20$ where crystals were observed within a few days, larger agregates were detected more frequently. Still, their relative mass and number was very low with a mass fraction of less than 0.1 %. Only in a small region of supersaturations (e.g. $c_P = 3.5$ mg/ml, 1.5 M sodium/potassium phosphate

buffer, pH 8.7, $\sigma \sim 35$), large particles were so abundant that their size could be determined with more confidence (fig. 9). At even higher concentrations of lumazine synthase, molecules aggregated too fast to be observed by dynamic light scattering. The aggregation pattern observed by dynamic light scattering almost only depended on supersaturation and a decrease in sodium/potassium phosphate concentration from 1.5 M to 1.45 M did not affect the onset of increased detection of aggregates.

To summarize, with lumazine synthase, no steady growth of aggregates was observed and the detected aggregates could not be assigned to the critical nucleus as it was the case for the three proteins mentioned above. To explain this discrepancy, the limitations of dynamic light scattering have to be considered first. To distinguish two monodisperse populations by dynamic light scattering, three conditions have to be fulfilled. First, the intensities of light scattered by the different populations have to be comparable. As a first approximation, the scattering intensity increases with the 6th power of radius. Thus, only few but very large particles can have the same scattering intensity as an abundant population of small particles. Next, the overall scattering intensity has to stay constant within the timeframe of one measurement. Therefore, growth should be negligible within a single measurement and the total number of scatterers should remain constant in the scattering volume. This can be a problem if one species is low in number but large in size. Third, the sizes have to differ significantly. As a rule of thumb, the size difference between two species needs to be about a factor of five or greater to obtain reliable resolution of particle size distributions (Wilson, 2003).

Prenucleation events Provided that the stock solutions were free from impurities and aggregates, only single lumazine synthase molecules should have been present directly after preparing the supersaturated solutions. Thus, prior to any nucleation event the particle size distribution should peak at the position of the single molecule. With increasing protein concentration, density fluctuations will amplify and the size distribution will shift and broaden marginally, but almost undetectable to dynamic light scattering due to the reasons listed above.

In agreement with this general scenario, almost all autocorrelation functions of lumazine synthase solutions recorded at lower supersaturation and prior to nucleation were best fitted by a single exponentially decaying function. A minor fraction of recorded autocorrelation functions deviated from the single exponential decay and revealed the presence of larger particles. Fig. 12 shows field autocorrelation functions acquired during different stages of crystallization. Curve A (black line) resembles the majority of all recorded autocorrelation functions, where only the single lumazine synthase molecules were found. The field autocorrelation function B (red line) illustrates the case, where a second population of larger species was detected. As can be seen, curve B differs only slightly from curve A and thus, the second population contributes little to the autocorrelation function B in fig. 12 and the calculated radius of in this case 1568 nm is unreliable.

Nonetheless, this second population is present and the question of its nature arises. A first assumption is the presence of "dust" or other impurities. This is very unlikely as solutions of lumazine synthase in 0.2 M sodium/potassium phosphate buffer, pH 8.7, prepared in the same way as the crystallizing protein solutions, did not show this pattern. Next, formation of amorphous

aggregates with a fractal structure was observed in supersaturated, but not necessarily crystal-forming lysozyme solutions (Georgalis et al., 1999; Umbach et al., 1998). If the formation of those aggregates is energetically allowed and thus gives rise to the second population, there exists no reason why nucleation and growth of those aggregates should cease. However, frequency and total number and mass of the aggregates did not increase with time. Third, the second population might be observed because of density fluctuations. If the mean radius of this second population is in the range of found values from 100 nm to more than a micrometer, then the particles should be larger than the critical nucleus and continue growing. In addition, they should be detectable by light microscopy and last should dissolve and grow slowly and thus contribute to the autocorrelation functions over longer time scales. In summary, none of the explanations is satisfactory and the real nature of the second population remains obscure.

Postnucleation events Once ordered aggregates reach a critical size, they continue growing. The frequency of this event, the nucleation rate, increases exponentially with supersaturation (section 1.1.2). Nucleation is a stochastic process and crystals nucleate and grow independently. Thus, the particle size distribution of growing crystals is very broad. When gravity exceeds Brownian motion because of high mass density, the crystals sediment.

At low nucleation rates, only few crystals grow in the volume observed by dynamic light scattering and they contribute to the autocorrelation functions as noise and, if larger, as number fluctuations. At high nucleation rates, crystals nucleate almost instantaneous without an detectable induction period, autocorrelation functions are quickly dominated by the large scatterers and

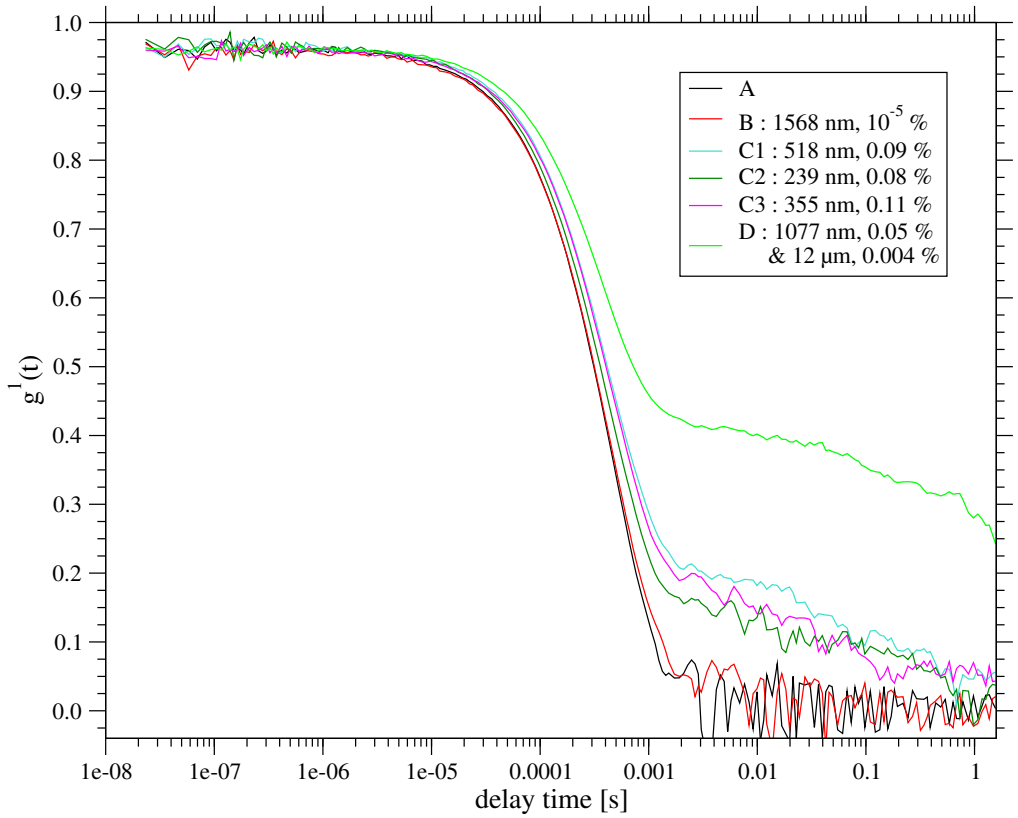

Figure 12: Field autocorrelation functions $g^1(t)$ at different stages of crystallization of lumazine synthase. Fitted radius and relative mass of aggregates are listed in the legend.

mean size increases. Lumazine synthase crystals grown in 1.5 M sodium/potassium phosphate buffer, pH 8.7, sediment very slowly because of the relative small density difference between solvent ($\rho \simeq 1.2$ g/cm^3) and protein ($\rho \simeq 1.36$ g/cm^3). Thus, very large but only few particles can interfere the spectra.

The time evolution of particle size distributions of lumazine synthase conforms with these predictions. At low protein concentration, aggregates were detected with increased frequency after an induction period that decreases with increasing supersaturation. In the case of the presented crystallization exper-

iment in 1.5 M sodium/potassium phosphate buffer with $c_P = 3$ mg/ml the induction time was about 10 hours (fig. 8). The corresponding autocorrelation functions resemble curve B in fig. 12, that was recorded within this induction time. At higher supersaturations, aggregates were detected almost instantaneously after mixing the protein and precipitant solutions. As the population of aggregates grew in size and mass, intensity of scattered light increased (see curves C1, C2 and C3 in fig. 12) and sizes varied less (fig. 9, blue bars, 18 min $<$ t $<$ 40 min). Within this period, an increase in the mean size was observed. Waiting longer, autocorrelation functions became dominated by huge particles so that the autocorrelation functions did not decay to zero within the period of a single measurement (curve D in fig. 12) and/or had values larger than one due to large number fluctuations. These particles might have been microcrystals as crystals were observed in the light microscope a few hours later.

Dynamic light scattering provides information about particle size distribution only and not about the type of scatterer. Thus, it is not certain that the detected aggregates are crystalline, especially as the formation of needle-like structures was observed at a slightly higher supersaturation of $\sigma = 40$ (fig. 10, $c_P = 4$ mg/ml, 1.5 M sodium/potassium phosphate, pH 8.7). Tanaka et al. (1999) for example reported the growth of aggregates with fractal dimensions in crystal-forming solutions and speculated that crystals were nucleated within those aggregates.

Comparison with other protein systems Crystals of lumazine synthase were grown within a few days only at very high supersaturations ($\sigma \geq 30$, $c_P \geq 3$ mg/ml in 1.5 M sodium/potassium phosphate buffer, pH 8.7). Normally, protein crystals are grown at much lower supersaturations. Typical

values range from 2 to 4 for apoferritin and pumpkin seed globulin (Malkin and McPherson, 1993a,b) and 6 to 12 for lysozyme (Drenth et al., 2003). Supersaturation was defined as the ratio of the actual activity of proteins in solution and the activity at equilibrium ($\sigma = a_P/a_E \simeq c_P/c_E$, eq. 3 in section 1.1.2). The activities can be replaced by the respective concentrations if the activity coefficient is almost equal to one. This is certainly not the case at the high salt concentrations employed for crystallization (Atkins, 1994). As already mentioned in section 2.1, the determination of protein concentration is less reliable at high phosphate and low protein concentration and thus, the determined solubility concentration may introduce an error. The uncertainty in supersaturation alone cannot explain the discrepancies in supersaturation necessary to nucleate crystals.

In the crystallization experiments presented by Malkin et al. (1993) and Malkin and McPherson (1993a,b), the protein stock solutions always contained aggregates. Many other proteins show significant protein aggregation as well after prolonged storage (Yoon et al., 2001). It is possible that the clusters are irregular aggregates of or around foreign protein or modified protein molecules (Chernov, 1997). They might act as seeds or at least promote formation of critical nuclei thereby lowering the nucleation barrier and enhancing nucleation rate. In the strict sense, this cannot be considered as homogeneous nucleation anymore.

For apoferritin it was shown that it forms oligomers (dimers, trimers, etc ...), probably induced by partly denaturation of the protein (Petsev et al., 2000). Compared to oligomer free preparations, oligomer containing solutions nucleate faster, whereas supersaturated microhomogeneous monomer solutions produce larger, better diffracting and less numerous crystals (Thomas et al., 1998).

Furthermore, it was speculated that higher oligomers (∼10 mer and ∼180 mer) may act as the nucleation centers observed by Malkin and McPherson (1993b).

To verify this, a crystallizing solution of microhomogeneous apoferritin monomers (section 4.1.3) was studied by dynamic light scattering at a protein concentration of 1 mg/ml in 0.2 M sodium acetate buffer, pH 5.0, containing 0.11 M cadmium sulfate (2.3 % (w,v)). No higher oligomers were detected and during crystal growth total intensity of scattered light decreased. Shape and morphology of the obtained crystals agreed with published results (Thomas et al., 1998).

It was shown that impurities (homologous or heterologous) are often present in protein solutions and thus can influence both crystal nucleation and crystal growth. In the majority of cases, the presence of aggregates is disadvantageous for crystal quality as mosaicity appearing at initial stages of crystal growth cannot heal at later stages of growth (Chernov, 2003).

In the case of lumazine synthase, very high supersaturations are needed to promote nucleation of crystals, which is generally known to be detrimental for crystal quality (Vekilov and Chernov, 2002). In addition, with increased supersaturation different solid phases, unstable with respect to the crystalline phase, but with a lower free energy than the protein solution, can form (Rosenberger et al., 1996). At lumazine synthase concentrations above 4 mg/ml in 1.5 M sodium/potassium phosphate buffer, pH 8.7, needle-like aggregates were formed besides crystals. The former might serve as nucleation sources or can even become incorporated into the crystals.

2.4 Metastable aggregates in supersaturated solutions of lumazine synthase

During the induction period, during wich no lumazine synthase crystals nucleated, a minor fraction of all recorded autocorrelation functions revealed the presence of a second population of aggregates besides the single molecules (first hours in fig. 8), whose nature could not be elucidated satisfyingly (section 2.3.3). All discussed experiments were conducted at high supersaturations and it can be assumed that the aggregates were detected only at conditions where crystals nucleate readily and the aggregates were first signals of crystals. Conversely, the second population was detected almost independently of salt concentration whereas its frequency increased with protein concentration.

Figs. 13 and 14 show the time evolution of the average sizes and relative masses of aggregates of lumazine synthase in 1.3 and 1.4 M sodium/potassium phosphate buffer, pH 8.7, respectively. After mixing protein stock solution and precipitating agent, preparations were filtered again through a 0.22 µm syringe filter to assure that aggregates formed during the mixing process due to high initial local supersaturations were removed. The reduction in protein concentration is marginal and can be neglected (section 4.3.1). Spectra were recorded at scattering angles of 60° and 90° consecutively from preparations that were successively diluted by the addition of buffer into the scattering cell. For these experiments the dynamic light scattering setup was aligned for a scattering angle of 90° and thus, the particle size distributions obtained at 60° were less reliable. Initial protein concentration of 6.5 mg/ml in the case of the 1.3 M sodium/potassium phosphate solution (red and black bars in fig. 13) was decreased to 3.2 mg/ml (not shown) and 2.3 mg/ml (blue bars). The 1.4 M so-

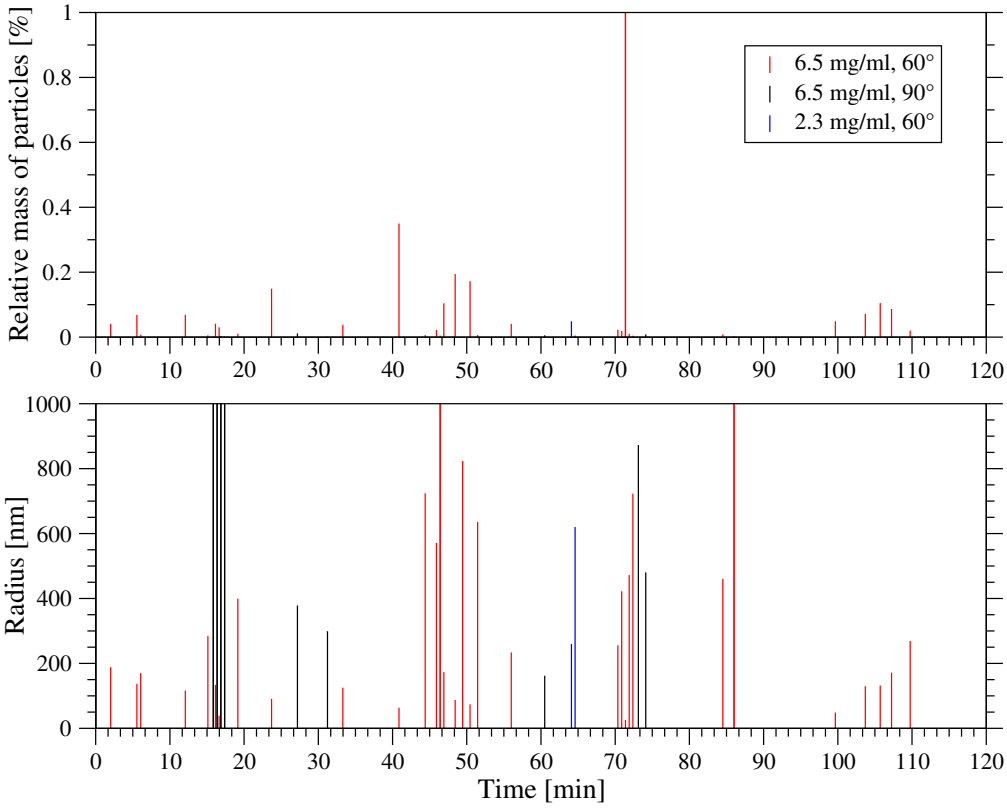

Figure 13: Time-resolved DLS: Time evolution of the average sizes and relative masses of aggregates of lumazine synthase in 1.3 M sodium/potassium phosphate buffer, pH 8.7. Protein concentration and scattering angle are listed in the legend. Monomers are not shown (R_h = 8 nm).

dium/potassium phosphate solution was diluted from 5 mg/ml (red and black bars in fig. 14) to 2.5 mg/ml after two days (blue bars) and 1.7 mg/ml (not shown).

The 1.3 M sodium/potassium phosphate solution with c_P = 6.5 mg/ml revealed the presence of a second population in 15 % of all autocorrelation functions recorded at 60°. The frequency decreased with decreasing protein concentration to 9 % at c_P = 3.2 mg/ml (not shown) and less than 1 % at c_P = 2.3 mg/ml. At a scattering angle of 90°, the same decrease in frequency

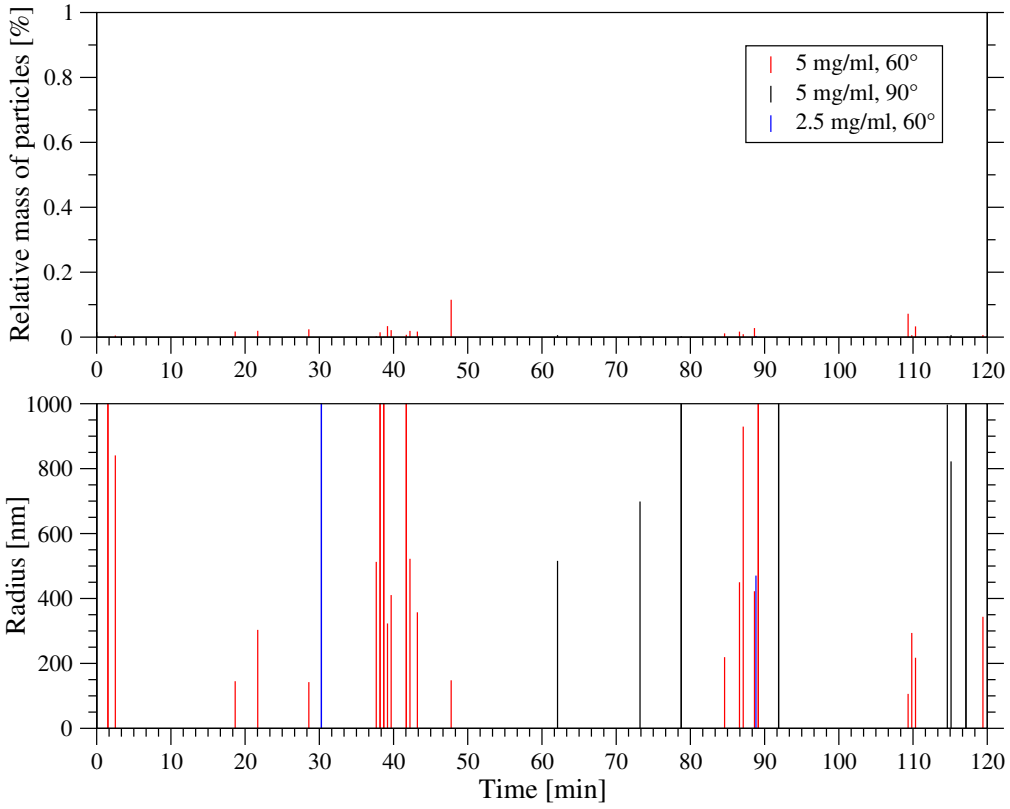

Figure 14: Time-resolved DLS: Time evolution of the average sizes and relative masses of aggregates of lumazine synthase in 1.4 M sodium/potassium phosphate buffer, pH 8.7. Protein concentration and scattering angle are listed in the legend. Monomers are not shown (R_h = 8 nm).

was observed whereas the initial frequency was lower than at 60°. In 5 % of all spectra, aggregates were detected at a protein concentration of 6.5 mg/ml and the frequency decreased to 4 % at c_P = 3.2 mg/ml (not shown) and 0 % at c_P = 2.3 mg/ml.

The protein solutions in 1.4 M sodium/potassium phosphate buffer, pH 8.7, showed essentially the same features (fig. 14). At a protein concentration of 5 mg/ml 10 % and 4 % of all recorded spectra at 60° (red bars) and 90° (black bars), respectively, revealed the presence of aggregates of lumazine synthase.

Decreasing the protein concentration to 2.5 mg/ml (blue bars) and 1.7 mg/ml (not shown) the autocorrelation functions were almost always best fitted by the single exponential decay of the single lumazine synthase molecule.

Besides a two-fold increased frequency, the aggregates had a higher mass fraction at a scattering angle of 60°. One reason is the small misalignment of the scattering setup at 60° and thus, an uncertainty in the wavevector **q** that affects the size and relative mass but not the frequency of observation of larger particles. If the size of the scattering particles is comparable to the wavelength of scattered light, the intensity of scattered light is angular dependent and decreases with increasing scattering angle. Due to the increased scattering volume of $1/\sin(60°)$ at 60° the recorded spectra should be less susceptible to number fluctuations than at a scattering angle of 90°.

In summary, in 1.3 –1.5 M sodium/potassium phosphate a second population of aggregates was always present besides monomeric lumazine synthase population. The former was observed more frequently by dynamic light scattering with increasing protein concentration. Whether and how this population is connected to crystal nucleation and or crystal growth cannot be addressed by dynamic light scattering alone.

The nature of this second population remains obscure. This issue was already addressed in section 2.3 and shall be discussed here in more detail. The second population was not observed in every single measurement and varied in size and mass. Thus, the number and/or the size of scatterers changed within the scattering volume. Correlation functions that are skewed by those fluctuations can at best give a rough estimate of size and amount of scatterers.

Without prior knowledge of solution preparation, this second population would be mistaken as “dust” that is a rather general term used to describe any

undesirable, large scatterers that contribute to the signal. However, all solutions were filtered prior to the dynamic light scattering experiments through 0.2 µm syringe filters and all particles larger than this size should be absent in the scattering cell. In addition, preparations in 0.2 M sodium/potassium phosphate buffer, pH 8.7, were all monodisperse. Evidently, this second population was present in detectable amounts only in supersaturated solutions and was not the result of "dust".

If the second population consisted of irregular aggregates around foreign protein or modified lumazine synthase molecules, it is difficult to explain why those aggregates were only seen in supersaturated solutions and not in low salt buffer. They might exist in low salt buffer, however due to their small size that leads to a negligible intensity of scattered light compared to the light scattered by the single lumazine synthase molecules, they cannot be detected. Nevertheless, in supersaturated solutions, these aggregates may act as seeds and may cause the agglomeration of lumazine synthase. With increasing size the intensity of scattered light increases and the aggregates become detectable.

But, if those aggregates exist and they grow in suppersaturated solutions, there exists no reason why this growth should cease. With time, the aggregates should sediment or at least should disturb the autocorrelation functions with increasing intensity.

With increasing protein concentration density fluctuations amplify and size distribution shifts to larger values. Classical nucleation theory (section 1.1.2) assumes that by successive aggregation of lumazine synthase molecules spherical clusters with crystalline structure are formed. Before reaching a critical size, the clusters dissolve faster than they grow. This critical size is unknown for crystallizing lumazine synthase and only limited data is available for other

protein crystallizing systems.

Malkin and McPherson (1993b) published that for crystallizing apoferritin solutions, the critical size R_h ranges between 20 nm and 26 nm at supersaturations from $\sigma = 2.5$ to 2.1, respectively. A compact spherical cluster would then contain about 30 to 65 apoferritin molecules. But the dynamic light scattering analysis showed also aggregates with similar size in solutions free of precipitating agent and thus, the results are of limited confidence (section 2.3.3, page 44). Nonetheless, atomic force microscopy studies were able to corroborate the determined dimensions, whereas the identified near-critical nuclei had a quasi-planar structure (Yau and Vekilov, 2000).

Critical nuclei for lysozyme crystals seemed to contain 10 or less molecules as determined independently by light microscopy (Galkin and Vekilov, 2000) and nuclear magnetic resonance spectroscopy (Drenth et al., 2003), irrespective of the underlying nucleation theorem, being classical (García-Ruiz, 2003) or model-independent (Oxtoby and Kashchiev, 1994).

The exact size of aggregates contributing to the second population in supersaturated lumazine synthase solutions is unknown. But, as the intensity of scattered light is angular dependent, the aggregates are larger than pure Rayleigh scatterers and their radius should at least be larger than $\lambda/20 = 33$ nm, as a rough estimate. The number of molecules in the nucleus is $n = V/v_0$, with V, the volume of the nucleus and $v_0 = 3.2 \cdot 10^3$ nm^3, the volume occupied by one molecule in the crystal, calculated from the volume of the unit cell of a hexagonal crystal of lumazine synthase and number of molecules within the unit cell (Schott et al., 1990). A compact spherical cluster would then consist of more than 47 lumazine synthase molecules. In the two presented experiments in 1.3 M and 1.4 M sodium/potassium phosphate

buffer, pH 8.7, the highest lumazine synthase concentrations used were 6.5 and 5 mg/ml and the supersaturations were $\sigma \approx 2.4$ and 9.1, respectively. Thus, with this size and number of growth units the clusters should already be post-critical and grow steadily at least in the case of the 1.4 M solution. Together with the different crystal nucleation and growth characteristics observed at high supersaturations by dynamic light scattering (section 2.3), density fluctuations of compact clusters disqualify as explanation for the larger particles detected at low and moderate supersaturations.

To grow crystals from solution, growth units have to orient themselves translationally and rotationally. Thus, the transition from liquid to solid phase occurs along two order parameters, density and structure. If these transitions do not proceed simultaneously and density fluctuations precede structural fluctuations, a dense unstructured aggregate state should form as an intermediate between liquid and solid phase. This mechanism was suggested by simulations for protein solution systems near their critical point for liquid-liquid phase separation (Lomakin et al., 2003; ten Wolde and Frenkel, 1997).

If such an unstructured dense intermediate is metastable in respect to the supersaturated protein solution, it is low in number and has a limited lifetime. Next, a "density-only-fluctuation" can produce particles larger than those produced by a coherent fluctuation of structure and density before a critical nucleus is formed. Thus, this model is compatible with the scattering signature observed at low supersaturations of lumazine synthase.

This finding was corroborated by atomic force microscopy studies carried out in the laboratory of Prof. Peter Vekilov at the University of Houston, Department of Chemical Engineering, Texas, USA. The growth of lumazine synthase crystals was monitored *in situ* in 1.3 sodium/potassium phosphate

buffer, pH 8.7, with protein concentrations ranging from 1 to 30 mg/ml. At protein concentrations of 3 mg/ml and higher, Gliko et al. (2005b) observed landing of 3D objects on the crystal surface with an approximate size of 100 to 160 nm (fig. 15a and 15g). The object shrinked in height (figs. 15g and h) and grew sideways. The 5 new growth layers orginating from the cluster in fig. 15b merged seamlessly with each other and with the underlying lattice without causing any lattice defects (figs. 15c – f). In addition, the new layers revealed the same growth kinetics as the other layers on the crystal surface. The probability of a microcrystal landing on a crystal surface in perfect registry with the underlying lattice would have been negligible and an unstructured solid aggregate would not have shrinked in size. Thus, the 3D-objects were identified as dense liquid droplets of lumazine synthase. At supersaturations of $\sigma < 3$ the liquid droplets were the only source of new growth layers.

It is evident that those dense liquid droplets of lumazine synthase must cause the aggregation pattern observed by dynamic light scattering. The droplets have a size that is comparable to the probe length $1/q$. Using as form factor $P(\mathbf{q}, R_h)$ that of hard spheres (eq. 16) and assuming a radius of 50 nm, the form factor decreases from 0.96 to 0.38 when increasing the scattering angle from 60° to 90°. This explains the difference in frequency of detection of aggregates at the two scattering angles.

$$P(\mathbf{q}, R_h) = \left[\frac{3}{(qR_h)^2} \left\{ \sin(qR_h) - qR_h \cos(qR_h) \right\} \right]^2 \tag{16}$$

In addition, the droplet population was not detected in every single measurement and consequently changed in number and/or size within the period of 30 s. The growth and dissolution rates of lumazine synthase crystals of

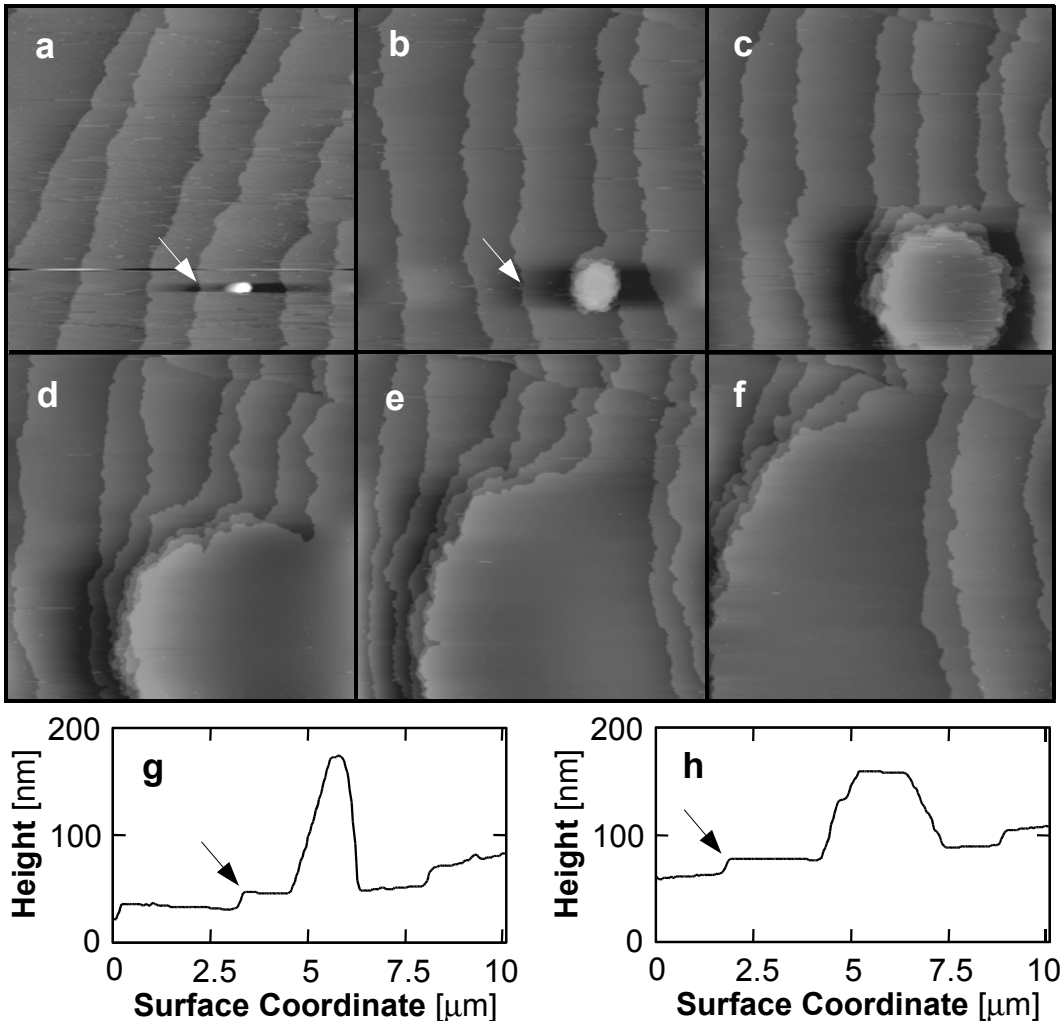

Figure 15: Tapping mode atomic force microscopy imaging of a crystal surface of lumazine synthase (001 face) in 1.3 M sodium/potassium phosphate buffer, pH 8.7, at c_P = 3 mg/ml. Scan size is 20×20 µm, the time interval between images is 9 min (Gliko et al., 2005b).
Sedimentation of a 3D object (a) onto a crystal surface of lumazine synthase and its development into a stack of five crystalline layers (b)-(f) in lumazine synthase solution of 3 mg/ml in 1.3 M sodium/potassium phosphate buffer, pH 8.7. Height profiles (g) and (h) along a horizontal line crossing the 3D-object in (a) and (b), respectively, show the object height of ∼120 nm directly after landing on the surface in (a) and ∼75 nm in (b) corresponding to 5 growth layers. Arrows in (a),(b),(g) and (h) mark the same step.

approximately 0.2 – 0.7 nm/s in 1.3 M sodium/potassium phosphate buffer at a supersaturation below $\sigma < 2.5$ (Gliko et al., 2005a,b) are not compatible with the fluctuations observed by dynamic light scattering whereas fast nucleation and growth and decay rates have been shown for dense liquid droplets in lysozyme solutions (Shah et al., 2004).

As the dense liquid droplets of lumazine synthase have a limited lifetime and do not grow to dimensions observable by light microscopy they have a higher free energy than both, the crystals and the protein solution. But the droplets are detectable by atomic force microscopy and dynamic light scattering and consequently, there must exist an energy barrier that hinders dissolution of the droplets and thus, the droplets are metastable with respect to the protein solution.

In the 1.3 M and the 1.4 M sodium/potassium phosphate buffer the droplets were detected more frequently with increased lumazine synthase concentration by dynamic light scattering, as increased protein concentrations amplify density fluctuations. Astonishingly, the amplification does not change when increasing the sodium/potassium phosphate concentration from 1.3 M to 1.4 M. However at the same time the solubility drops from 2.7 mg/ml to 0.55 mg/ml and the supersaturation increases.

3 Conclusion

Lumazine synthase crystallizes in sodium/potassium phosphate buffer, pH 8.7. In this study it was found that its solubility decreases from 7 mg/ml to less than 0.1 mg/ml increasing salt concentration from 1.2 to 1.55 M (section 2.1). Contrary to that change, the determined osmotic second virial coefficient of lumazine synthase, a parameter to quantify particle interactions, remains almost invariant to the increase in salt concentration (section 2.2). It is almost zero at the storage conditions (0.2 and 0.9 M sodium/potassium phosphate buffer, pH 8.7) and at salt concentrations where lumazine synthase crystallizes readily (1.3 and 1.4 M). Thus, compared to a system of hard spheres the interactions are always slightly attractive. On the other hand, most other protein systems characterized in terms of the second virial coefficient showed a distinct change when adding precipitant to protein solutions and revealed substantially lower values of the second virial coefficient at crystallization conditions.

One possible explanation of the observed discrepancy between measured 2nd virial coefficient and observed crystallization behavior is an interplay of expected attractive short-range potential and longer-range repulsive potential caused by solvent structuring at high salt concentrations (section 2.2.2). Structured solvent or higher solvent density at the protein-solvent interface due to lower mobility of structured solvent can be detected by small angle neutron scattering utilizing the difference in scattering cross section of solvent (sodium/potassium phosphate in H_2O and D_2O) and protein and hence, should be subject of further investigations. In addition, the envisioned potential landscape exhibiting repulsive and attractive character is accessible in principal by measuring the structure factor over a wide q-range as possible by small-angle

x-ray and neutron scattering.

In search of protein clusters, crystal forming or amorphous, solutions of lumazine synthase were thoroughly studied by dynamic light scattering in a broad range of supersaturations (section 2.3). As predicted by the nucleation theory, increased supersaturation facilitated nucleation of crystals that was accompanied by an increased frequency of detection of aggregates. However, sizes of aggregates ranged from 100 nm to several micrometers, the relative mass fraction of aggregates was very low and almost no growth of aggregates in size and increase in mass was observed. In addition, the onset of increased detection of aggregates was not well defined and crystallization experiments under virtually unchanged conditions always yielded different aggregation patterns and consequently their induction time could not be determined.

These difficulties in assessment of aggregation behavior are caused by the fluctuation of number and/or mass of scattering aggregates in the scattering volume manifested in the variation of determined average size and mass of aggregates within the acquisition time of an autocorrelation function (30 s). With increasing size of the scatterers, presumably microcrystals, uncorrelated intensity fluctuations dominated the recorded spectra and calculated particle size distributions were deemed unreliable.

To image the lumazine synthase clusters linked to crystal growth, supersaturated solutions were analyzed by cryo transmission electron microscopy (section 2.3.2). The electron micrographs exhibited a network of lumazine synthase molecules. However, the molecules were difficult to identify and it was not possible to discern whether molecules were interconnected or not. In addition, lumazine synthase clusters with a linear arrangement were observed at higher supersaturations where aggregates were detected by dynamic light

scattering almost immediately after starting the crystallization experiments inferring they might be near-critical aggregates. The sizes of aggregates determined by electron microscopy and light scattering could be roughly correlated, but the numerical proportion of aggregates to single molecules did not match. Furthermore, the solvent evaporated during preparation of the cryo samples and therefore the results have to be considered with caution.

Aggregates were also detected by dynamic light scattering in supersaturated solutions of lumazine synthase where nucleation of crystals is unlikely (section 2.4) in contrast to lumazine synthase at storage conditions. Average size and mass of aggregates did fluctuate as the aggregates were detected only in a small fraction of all recorded autocorrelation functions whereas the frequency of detection did not vary with time. In connection with atomic force microscopy studies carried out in the laboratory of Prof. Peter Vekilov at the University of Houston, Department of Chemical Engineering, Texas, USA, these aggregates were identified as dense liquid droplets of lumazine synthase metastable in respect to the protein solution and the crystal phase.

The formation of droplets of lysozyme due to an interplay of attractive and repulsive interactions was detected by measurement of the structure factor by combined small-angle x-ray and neutron scattering studies and interpretation of the determined "Bragg reflections" in terms of preferred interparticle distances (Stradner et al., 2004). To further substantiate and characterize the metastable droplets of lumazine synthase, in future studies the structure factor should be determined at low and high sodium/potassium phosphate concentrations as well.

Still unknown is whether the metastable droplets are involved in the nucleation of crystals at higher supersaturations or if the birth of lumazine synthase

crystals conforms to the classical nucleation theory of formation of nuclei with crystal like structure. As the metastable droplets gave rise to an angular dependency in the light scattering measurements and hence were detected with higher frequency at smaller scattering angles, change in size and number of this population at nucleation conditions should be observable by small angle dynamic light scattering measurements.

4 Materials and Methods

4.1 Biochemical methods

4.1.1 Chemicals

All chemicals were purchased from Sigma-Aldrich if not mentioned otherwise. For all preparations Milli-Q grade water (Millipore) was used and the solutions were filtered through 0.22 µm syringe filters (Millipore).

4.1.2 Expression and purification of lumazine synthase

Lumazine synthase from *B. subtilis* was overexpressed in recombinant *B. subtilis* strain BR151[pBL1]-p602-BS-ribH (Haase, 2002). Cells were grown in Luria-Bertani medium (10 g/l casein, 5 g/l yeast extract, 5 g/l sodium chloride) containing kanamycin (20 mg/ml) and erythromycin (15 mg/ml) at 32 ℃. At an OD_{600nm} of about 0.6–0.8, IPTG was added to a final concentration of 2 mM. Upon incubation for 18 h, the cells were harvested by centrifugation (GS3-rotor, Sorvall, 5,000 rpm, 20 min, 4 ℃), washed with 0.9 % (w/v) NaCl and stored at -20 ℃.

Frozen cells were suspended in a lysis buffer (20 mM potassiuphosphate, 10 mM Na_2SO_3, 10 mM EDTA, pH 7.0) containing 1 mg/ml lysozyme, 1 mM PMSF and 0.02 mg/ml DNAse. Upon incubation for 30 min at 37 ℃, the suspension was cooled on ice, sonified (B-12A, Branson SONIC Power Company) and centrifuged (70 Ti rotor, Beckmann, 45,000 rpm, 4 ℃, 1 h). The filtered supernatant (filter pore size 0.45 µm) was loaded on a Q-Sepharose anion-exchange chromatography column (Amersham Biosciences) equilibrated with 20 mM potassium phosphate buffer, pH 7.0. The column was eluted with a lin-

ear gradient of 0.02 – 1 M potassium phosphate at a flow rate of 3 ml/min. Protein containing fractions were analyzed by SDS-PAGE (section 4.1.5), pooled and concentrated by ultracentrifugation (70 Ti rotor, Beckmann, 32,000 rpm, 4 ℃, 16 h). The concentrated protein solution was dialyzed overnight at 4 ℃ against 0.2 M sodium/potassium phosphate buffer, pH 8.7, containing 1 mM 5-nitro-6-ribitylamino-2,4(1H,3H)-pyrimidinedione. The protein was further purified by crystallization with sodium/potassium phosphate (final concentration 1.5 M, pH 8.7) and subsequently stored in 0.2 M sodium/potassium phosphate buffer, pH 8.7, containing 300 µm 0.5-nitro-6-ribitylamino-2,4(1H,3H)-pyrimidinedione at 4 ℃.

4.1.3 Purification of apoferritin

Horse spleen apoferritin was obtained from Sigma Aldrich. The solution was dialyzed overnight at 4 ℃ against 0.2 M sodium acetate buffer, pH 5.0. Separation of monomers from aggregated appoferritin was done by gel filtration using a Hiload 16/60 Superdex 200 prep grade column (Amersham Biosciences). The mobile phase was 0.2 M sodium acetate solution at pH 5.0 at a flow rate of 0.5 ml/min. Protein containing fractions were analysed by native PAGE (section 4.1.5). Using this method monomers, dimers and higher oligomers could be separated. The size of monomers and dimers was verified by dynamic light scattering (section 4.3.2) and the measured sizes agreed well with published data (Hempstead et al., 1997; Petsev et al., 2001) showing radii of 6.4 and 9.7 nm for monomers and dimers, respectively.

4.1.4 Protein concentration determination

Protein concentration was determined using the Bradford analysis (Bradford, 1976) that is based on the shift of the absorption maxium of the dye Brilliant Blue G from 465 to 595 nm upon protein binding. The assays were performed with the Bio-Rad Protein Assay (Bio-Rad Laboratories GmbH) in a Ultrospec 1000 spectrophotometer (Amersham Biosciences) using bovine serum albumin (BSA) (SERVA Electrophoresis GmbH) as standard in the range from 0.05 to 0.6 mg/ml.

4.1.5 Gel-electrophoresis

SDS-PAGE and protein staining were performed according to Laemmli (1970). 16 % SDS-polyacrylamide gels (table 4) were prepared in a Miniprotean II electrophoresis unit (Bio-Rad Laboratories GmbH). Samples (5 µl) were heated to 100 ℃ for 3 min in 20 µl sample buffer (500 mM Tris-HCl pH 6.8, 20 % glycerol, 2 % SDS, 2 mM DTT, 0.1 % bromophenol blue) before loading. Gels were run at 20 mA per gel in electrophoresis buffer (25 mM Tris-HCl pH 8.3, 192 mM glycine, 0.1 % SDS). The run was stopped when the bromophenol blue reached the bottom of the gel. The gel was stained with Coomassie Brilliant Blue (0.1 % (w/v)) in 30 % methanol and 10 % acetic acid for 30 min. Excess dye was removed with a mixture of 30 % methanol and 10 % acetic acid.

Native-PAGE (5 % polyacrylamide gels, no stacking gel) and staining were performed as described for SDS-PAGE replacing all SDS fractions with water.

	Sperating gel 16 % acrylamide	Stacking gel 4 % acrylamide
Water	2 ml	3 ml
0.5 M Tris-HCl, pH 6.8		1.25 ml
1.5 M Tris-HCl, pH 8.8	2.5 ml	
30 % acrylamide (Bio-Rad)	5.3 ml	0.670 ml
10 % (w/v) SDS	0.1 ml	50 µl
TEMED (Fluka)	5 µl	5 µl
10 % (w/v) APS	50 µl	25 µl

Table 4: Composition of SDS-polyacrylamide gels.

4.2 Crystallization method

For the solubility determination of lumazine synthase, protein solutions were supersaturated by adding 4 M sodium/potassium phosphate buffer, pH 8.7, to the protein stock solutions. All other crystallization experiments were performed in batch mode by adding equal volumes of precipitating agent to protein stock solution (section 4.1.2 and 4.1.3). Prior to crystallization, all solutions were centrifuged (GS-15R Beckmann, 15,400 rpm, 30 min, 4 ℃) and filtered through 0.22 µm syringe filters (Millipore). During all crystallization experiments the temperature was maintained at 20 ℃, unless otherwise noted.

4.3 Light scattering

4.3.1 Static light scattering

Light scattering detector The static light scattering experiments were performed on a DAWN EOS (Wyatt Technology) that is coupled with a Shodex RI-71 refractive index detector (Showa Denko). The light scattering detector is equipped with a diode laser (30 mW, $\lambda = 690$ nm) and the scattered light is recorded at eighteen different angles using ASTRA (version 4.90.07, Wyatt

Technology).

The scattering cell is designed to be used as a flow cell. Due to its small size (volume = 0.07 µl, diameter = 1 mm), it is very sensitive to the presence of air bubbles and it proved useful to filter the solutions (0.22 µm syringe filters, Millipore Co.) during injection into the cell. The possible effect of reduction in protein concentration was tested by the Bradford assay (section 4.1.4). The effect was found to be marginal and within the error of the method (±10 %). Thus, for calculation of the molar mass and the second virial coefficient the unchanged concentrations were used.

Refraction index increment The refractive index increment (dn/dc) was measured using a Shodex RI-71 (Showa Denko) operating with a tungsten lamp (white light).

4.3.2 Dynamic light scattering

Dynamic light scattering setup All dynamic light scattering measurements were carried out in 8 mm cylindrical borosilicate cuvettes (Carl-Roth) using an Axios-150 instrument (Triton-Hellas). It is a fiber optic based instrument using a 35 mW diode laser with a wavelength of 658 nm. The detectors angular range is between 15° and 165° and the temperature can be controlled from 5 ℃ to 70 ℃. The digital correlator uses 288 channels spanning delay times from 11.64 ns to 56 min.

Spectra were recorded at 20 ℃ every 30 s at an angle of 60° for at least 2 hours unless otherwise noted. The particle size distributions were obtained from the autocorrelation functions using Provencher's regularized Laplace inversion CONTIN (Provencher, 1982a,b). Due to the unknown morphology of

the aggregates the form factors were approximated by those of hard spheres.

Dynamic light scattering data analysis This paragraph is a brief review on the light scattering theory. Further information is available in several textbooks (Pecora, 1985; Schmitz, 1990).

The light detected in a scattering experiment originates from the superposition of complex amplitudes due to scattering by many particles. As the particles in solution are buffeted by Brownian forces, the contributions have random time-dependent phases and total intensity of scattered light fluctuates as a function of time. In dynamic light scattering experiments, these fluctuation are quantified by temporal correlation of the intensity of scattered light $I(t)$:

$$g^2(\tau) = \langle I(t)I(t+\tau)\rangle = \langle I\rangle^2 + \langle \delta I(t)\delta I(t+\tau)\rangle \tag{17}$$

τ is the experimental delay time and $\delta I(t)$ the fluctuation about the average intensity $\langle I\rangle$. The intensity autocorrelation function $g^2(\tau)$ can be expressed in terms of the autocorrelation function, $g^1(\tau)$, of the scattered electric field, $E(t)$, according to the Siegert's theorem (equation 19).

$$g^1(\tau) = \langle E(t)E^*(t+\tau)\rangle \tag{18}$$

$$g^2(\tau) = \left|g^1(0)\right|^2 + \beta\left|g^1(\tau)\right|^2 \tag{19}$$

$g^1(0)$ is the average intensity of scattered light $\langle I\rangle$ and $\beta \leq 1$ is a constant that reflects the degree of spatial coherence of the detected light. The area of the detector is described by a range of wave vectors and the superposition of these different uncorrelated waves reduces the total correlation.

For small particles compared to the wavelength, the field autocorrelation

function is expressed as:

$$g^1(\mathbf{q},\tau) = \left\langle \sum_{i=1}^{N}\sum_{i=1}^{N} b_i b_j^* \mathrm{e}^{i\mathbf{q}\cdot\mathbf{r_i}(t)-i\mathbf{q}\cdot\mathbf{r_j}(t+\tau)} \right\rangle \tag{20}$$

with b_i and $\mathbf{r_i}$ the scattering intensity and position of the i^{th} particle. $\mathbf{q}$ is the wave vector with a magnitude of $q = (4\pi n_0/\lambda)\cdot sin(\theta/2)$. For free diffusing particles, their movements are statistically independent and eq. 20 reduces to:

$$g^1(\mathbf{q},\tau) = \sum_{i=1}^{N} \left\langle |b_i|^2 \mathrm{e}^{i\mathbf{q}\cdot\triangle\mathbf{r_i}(t,\tau)} \right\rangle \tag{21}$$

The displacement $\triangle\mathbf{r_i}(t)$ is a random variable and its exact behavior cannot be predicted. However, based on the theory of Brownian motion, the probability $G(\mathbf{r},t)d\mathbf{r}$ that a particle is located in the volume element $d\mathbf{r}$ at $\mathbf{r}$ at a time t is given by the diffusion eq. 22, Fick's 2nd law of diffusion, with the condition that the particle was initially located at the origin (eq. 23).

$$\frac{\partial G(\mathbf{r},t)}{\partial t} = D\nabla^2 G(\mathbf{r},t) \tag{22}$$

$$G(\mathbf{r},0) = \delta(\mathbf{r}) \tag{23}$$

The probability can be used to convert the time average needed in eq. 21 to a weighted average over all positions.

$$\left\langle e^{i\mathbf{q}\cdot\triangle\mathbf{r}(t,\tau)} \right\rangle = F(\mathbf{q},\tau) = \int d\triangle\mathbf{r}\, \mathrm{e}^{i\mathbf{q}\cdot\triangle\mathbf{r}} G(\triangle\mathbf{r},\tau) \tag{24}$$

$F(\mathbf{q},\tau)$ is then the Fourier transform of $G(\triangle\mathbf{r},\tau)$. By taking the Fourier

transform of eq. 22, following differential equation is obtained

$$\frac{\partial F(\mathbf{q},\tau)}{\partial \tau} = -q^2 D F(\mathbf{q},\tau) \tag{25}$$

whose solution is

$$F(\mathbf{q},\tau) = \mathrm{e}^{-q^2 D \tau}. \tag{26}$$

Combining the eqs. 21, 24 and 26, $g^1(\mathbf{q},\tau)$ is recast as:

$$g^1(\mathbf{q},\tau) = \sum_{i=1}^{N} \left\langle |b_i|^2 \right\rangle \mathrm{e}^{-q^2 D_i \tau} \tag{27}$$

In monodisperse preparations, all diffusion coefficients D_i are identical and the normalized field autocorrelation function is:

$$g^1(\mathbf{q},\tau) = \frac{g^1(\mathbf{q},\tau)}{g^1(\mathbf{q},0)} = \mathrm{e}^{-q^2 D_0 \tau} \tag{28}$$

From the decay time of a single exponential autocorrelation function the single particle diffusion coefficient D_0 and via the Stokes-Einstein relation (eq. 29) the hydrodynamic radius of spherical particles can be determined. η is the viscosity of the solvent.

$$D_0 = \frac{k_B T}{6\pi\eta R_h} \tag{29}$$

For dilute polydisperse systems, the intensity of the scattered light is the sum of the light scattered by the individual particles. The field autocorrelation function may be formulated as the Laplace transform of the distribution function $f(\gamma)$ of the decay rate γ, being a function of the diffusion coefficient.

θ	15°	30°	45°	60°	75°	90°
q [10^{-3} nm^{-1}]	3.3	6.6	9.7	12.7	15.5	18.0
θ	105°	120°	135°	150°	165°	180°
q [10^{-3} nm^{-1}]	20.2	22.1	23.5	24.6	25.3	25.5

Table 5: Magnitude of the wave vectors $q = (4\pi n_0/\lambda) \cdot sin(\theta/2)$ in the angular range accessible by the employed light scattering setup. Wavelength of laserlight is $\lambda = 658$ nm and refraction index is that of water ($n_0 = 1.334$).

$$g^1(\tau) = \int_0^\infty d\gamma\, f(\gamma) \mathrm{e}^{-\gamma\tau} \tag{30}$$

The distribution function $f(\gamma)$ can be recovered from the inversion of the Laplace transform. No more than 2 or 3 components can be resolved with confidence. For particles with sizes comparable to the wavelength, interacting particles and non-spherical particles, the form factor and structure factor have to be known and rotational diffusion has to be taken into account respectively.

If the dimensions of the scattering particle are comparable to the probe length $1/q$, then the amplitude of the incident light will differ for various regions within the particle. The phase differences lead to q-dependent interference effects in the intensity of scattered light and b_i is then a function of q. Table 5 lists the wave vectors in aqueous solutions accessible by the light scattering setup employed.

If the interactions between particles are significant, their trajectories are correlated and the off-diagonal terms in the double sum in eq. 20 do not vanish. It is not possible yet to fully predict the impact of this correlation in delay time τ and wavevector $\mathbf{q}$.

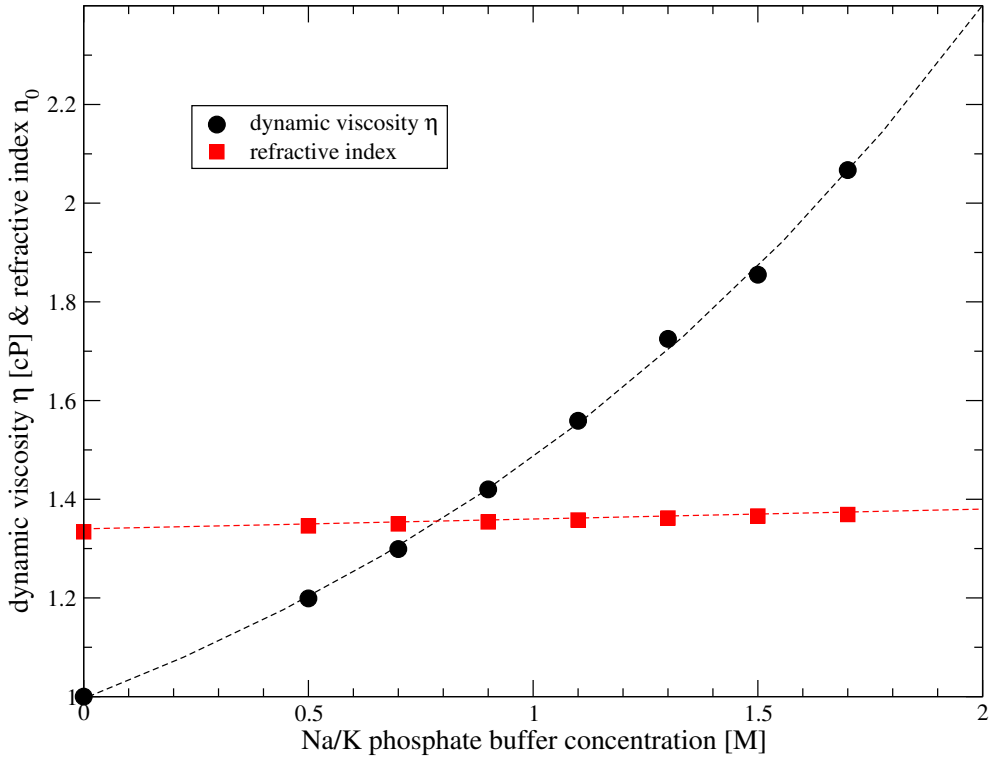

Figure 16: Refractive index and dynamic viscosity for different sodium/potassium phosphate buffers, pH 8.7. Lines are guides for the eye.

Refractive index and dynamic viscosity Because of the high sodium/potassium phosphate concentrations used in the crystallization experiments, the index of refraction and the dynamic viscosity cannot be approximated by that of water ($n_{\text{white light}} = 1.33$ and $\eta = 1.002\,\text{cP}$). The refractive indices were measured with an Abbé refractometer (Zeiss). The dynamic viscosities were determined from the kinematic viscosities measured with a V10 viscosimeter (Lauda Messgeräte) employing a Ubbelohde viscosimeter of size 0c (Schott-Geräte GmbH). The densities were measured with a pycnometer. The results are listed in table 6 and fig. 16.

	Na/K phosphate, pH 8.7 [M]						
c [M]	0.5	0.7	0.9	1.1	1.3	1.5	1.7
ρ [g/cm^3]	1.066	1.093	1.117	1.143	1.170	1.195	1.218
η [cP]	1.199	1.299	1.420	1.559	1.725	1.855	2.067
n_0	1.346	1.350	1.354	1.358	1.362	1.366	1.369

Table 6: Density ρ, dynamic viscosity η and refractive index n_0 of different sodium/potassium phosphate buffers, pH 8.7, with concentration c.

4.4 Microscopy

4.4.1 Light microscopy

For light microscopy, an Axioskope 2 (Zeiss) with 20× and 40× objectives was used in phase contrast or differential interference contrast mode. Images were recorded with a photo adaptor (MPS 45 and MPS 51, Wild Heerbrugg) on Agfapan APX 400 films, which were developed for 7 minutes at room temperature in Rodinal B&W film developer (Kodak).

Temperature control A temperature controlled stage was built in-house for the Axioskop 2 to observe growth or dissolution of lumazine synthase crystals at different temperatures. The stage was constructed as a hollow cylinder with width and height of 6.5 cm and 0.9 cm, respectively, built out of aluminium, whose temperature was controlled by a MultiTemp III water cooling system (Amersham Biosciences) within a temperature range from 4 °C to 90 °C. The object slide with the sample was placed on the cylinder that contained a hole with a diameter of 2 cm to illuminate and observe the sample. For thermal insulation the object slide was covered with a sheet of neoprene of 1 mm thickness. Because of the low thermal conductivity of the object slide of approximately 1 $Wm^{-1}K^{-1}$ there was always a temperature difference between

sample and the cylinder. Therefore, the temperature was always measured at the position of the sample on the object slide.

4.4.2 Cryo transmission electron microscopy

For cryo transmission electron microscopy (cryo-TEM), 4 µl drops of lumazine synthase solution were placed on holey carbon grids (2 µm hole size, Quantifoil), blotted and plunged into liquid ethane (T = -182 ℃). The cooling rate of approximately 10^6 K/s ensured that samples solidified in vitreous state without the formation of ice crystals.

Cryo samples were transfered with a cryo-holder from Gatan to a Jeol 2010 transmission electron microscope equipped with a LaB_6 filament and operating at an acceleration voltage of 120 kV. Micrographs were recorded at a magnification of 50,000 on Kodak SO 163 negatives that were developed in full-strength D19 developer (Kodak) for 12 minutes at room temperature.

Only areas of frozen solution free of support were examined, ensuring that no adsorption artifacts were recorded. The ice layer had a thickness of approximately 200 nm.

References

P.W. Atkins. *Physical Chemistry.* Freeman, 5th edition, 1994.

A. Bacher, R. Baur, U. Eggers, H.-D. Harders, M.K. Otto, and H. Schnepple. Riboflavin synthases of *Bacillus Subtilis*. *J. Biol. Chem.*, 255(2):632–637, 1980.

A. Bacher, M. Fischer, K. Kis, K. Kugelbrey, S. Mörtl, J. Scheuring, S. Weinkauf, S. Eberhardt, K. Schmidt-Bäse, R. Hubert, K. Ritsert, M. Cushman, and R. Ladenstein. Biosynthesis of riboflavin: structure and mechanism of lumazine synthase. *Biochem. Soc. Trans.*, 24:89–94, 1996.

V. Ball and J.J. Ramsden. Buffer dependence of refractive index increments of protein solutions. *Biopol.*, 46:489–492, 1998.

P. Bénas, L. Legrand, and M. Riès-Kautt. Strong and specific effects of cations on lysozyme chloride solubility. *Acta Cryst. D*, 58:1582–1587, 2002.

T.L. Blundell, H. Jhoti, and C. Abell. High-throughput crystallography for lead discovery in drug design. *Nat. Rev. Drug. Discov.*, 1:45–54, 2002.

F. Bonneté and D. Vivarès. Interest of normalized second virial coefficient and interaction potentials for crystallizing large macromolecules. *Acta Cryst. D*, 58:1571–1575, 2002.

M. Boström, D.R.M. Williams, and B.W. Ninham. Why the properties of proteins in salt solutions follow a Hofmeister series. *Curr. Opin. Colloid Interface Sci.*, 9:48–52, 2004.

M.M. Bradford. A rapid and sensitive method for the quantitation of microgram quantities of protein utilizing the principle of protein-dye binding. *Analyt. Biochem.*, 72:248–254, 1976.

N. Braun, J. Tack, M. Fischer, A. Bacher, L. Bachmann, and S. Weinkauf. Electron microscopic observations on protein crystallization: adsorption layers, aggregates and crystal defects. *J. Cryst. Growth*, 212:270–282, 2000.

M. Casselyn, J. Perez, A. Tardieu, P. Vachette, Witz J., and H. Delacroix. Spherical plant viruses: interactions in solution, phase diagrams and crystallization of brome mosaic virus. *Acta Cryst. D*, 57:1799–1812, 2001.

D. Chandler. *Introduction to modern statistical mechanics*. Oxford Unversity Press, 1987.

N.E. Chayen. Turning protein crystallisation from an art into a science. *Curr. Opin. Struct. Biol.*, 14:577–583, 2004.

A.A. Chernov. Crystals built of biological macromolecules. *Phys. Rep.*, 288: 61–75, 1997.

A.A. Chernov. Protein crystals and their growth. *J. Struct. Biol.*, 142:3–21, 2003.

A.A: Chernov. Notes on the interface growth kinetics 50 years after Burton, Cabrera and Frank. *J. Cryst. Growth*, 264:499–518, 2004.

A.A. Chernov and L.J. DeLucas. View on biocrystallization from Jena, 2002. *Acta Cryst. D*, 58:1511–1513, 2002.

A.M. Davis, S.J. Teague, and G.J. Kleywegt. Application and limitations of X-ray crystallographic data in structure-based ligand and drug design. *Angew. Chem. Int. Ed.*, 42:2718–2736, 2003.

J. Drenth. *Principles of Protein X-ray Crystallography.* Springer, 1994.

J. Drenth, K. Dijkstra, C. Haas, J. Leppert, and O. Ohlenschläger. Effect of molecular anisotropy on the nucleation of lysozyme. *J. Phys. Chem. B*, 107: 4203–4207, 2003.

A. Ducruix, J.P. Guilloteau, M. Riès-Kautt, and A. Tardieu. Protein interactions as seen by solution x-ray scattering prior to crystallogenesis. *J. Cryst. Growth*, 168:28–39, 1996.

S.A. Edwards and D.R.M. Williams. Hofmeister effects in colloid science and biology explained by dispersion forces: analytic results for the double layer interaction. *Curr. Opin. Colloid Interface Sci.*, 9:139–144, 2004.

G.D. Fasman, editor. *Handbook of Biochemistry and Molecular Biology, Proteins, Vol. II.* CRC Press, Cleveland, OH, 3rd edition, 1976.

G. Feher and Z. Kam. Nucleation and growth of protein crystals: general principles and assays. *Methods Enzymol.*, 114:77–112, 1985.

S. Finet, F. Bonneté, J. Frouin, K. Provost, and A. Tardieu. Lysozyme crystal growth, as observed by small angle x-ray scattering, proceeds without crystallization intermediates. *Eur. Biophys. J.*, 27:263–271, 1998.

S. Finet, F. Skouri-Panet, M. Casselyn, F. Bonneté, and A. Tardieu. The Hofmeister effect as seen by SAXS in protein solutions. *Curr. Opin. Colloid Interface Sci.*, 9:112–116, 2004.

O. Galkin and P.G. Vekilov. Are nucleation kinetics of protein crystals similar to those of liquid droplets? *J. Am. Chem. Soc.*, 122:156–163, 2000.

O. Galkin and P.G. Vekilov. Nucleation of protein crystals: critical nuclei, phase behaviour, and control pathways. *J. Cryst. Growth*, 232:63–76, 2001.

J.M. García-Ruiz. Arcade games for teaching crystal growth. *J. Chem. Educ.*, 76:499–501, 1999.

J.M. García-Ruiz. Nucleation of protein crystals. *J. Struct. Biol.*, 142:22–31, 2003.

J.M. García-Ruiz, M.L. Novella, and F. Otálora. Supersaturation patterns in counter-diffusion crystallisation methods followed by Mach-Zehnder interferometry. *J. Cryst. Growth*, 196:703–710, 1999.

Y. Georgalis and W. Saenger. Light scattering studies on supersatured lysozyme solution. *Cryst. Growth. Res.*, 4:1–62, 1998.

Y. Georgalis, P. Umbach, W. Saenger, B. Ihmels, and D.M. Soumpasis. Ordering of fractal clusters in crystallizing lysozyme solutions. *J. Am. Chem. Soc.*, 121:1627–1635, 1999.

A. George and W.W. Wilson. Predicting protein crystallization from a dilute solution property. *Acta Cryst. D*, 50:361–365, 1994.

J.W. Gibbs. On the equilibrium of heterogeneous substances. *Trans. Connect. Acad. Sci.*, pages 108–248, 1876.

J.W. Gibbs. On the equilibrium of heterogeneous substances. *Trans. Connect. Acad. Sci.*, pages 343–524, 1878.

J.W. Gibbs. *The Scientific Papers of J. Willard Gibbs*. Ox Bow Press, 1993.

O. Gliko, N. Neumaier, M. Fischer, I. Haase, A. Bacher, S. Weinkauf, and P. Vekilov. Dense liquid droplets as step source for the crystallization of lumazine synthase. *J. Cryst. Growth*, 275:1409–1416, 2005a.

O. Gliko, N. Neumaier, P. Weichun, I. Haase, M. Fischer, A. Bacher, S. Weinkauf, and P. Vekilov. A metastable prerequisite for the growth of lumazine synthase crystals. *J. Am. Chem. Soc.*, 127(10):3433–3438, 2005b.

J.-P. Guilloteau, M.M. Riès-Kautt, and A.F. Ducruix. Variation of lysozyme solubility as a function of temperature in the presence of organic and inorganic salts. *J. Cryst. Growth*, 122:223–230, 1992.

B. Guo, S. Kao, H. McDonald, A. Asanov, L.L. Combs, and W.W. Wilson. Correlation of second virial coefficients and solubilities useful in protein crystal growth. *J. Cryst. Growth*, 196:424–433, 1999.

C. Haas, J. Drenth, and W.W. Wilson. Relation between the solubility of proteins in aqueous solutions and the second virial coefficient of the solution. *J. Phys. Chem. B*, 103:2808–2811, 1999.

I. Haase. *Biosynthese von Vitamin B_2. Die Lumazinsynthase: Charakterisierung und Anwendung*. PhD thesis, Technische Universität München, 2002.

P.D. Hempstead, S.J. Yewdall, A.R. Fernie, D.M. Lawson, P.J. Artymiuk, D.W. Rice, G.C. Ford, and P.M. Harrison. Comparison of the three-dimensional structures of recombinant human H and horse L ferritins at high resolution. *J. Mol. Biol.*, 268:424–448, 1997.

J. Israelachvili and H. Wennerström. Role of hydration and water structure in biological and colloidal interactions. *Nature*, 379:219–225, 1996.

J.N. Israelachvili. *Intermolecular and Surface Forces.* Academic Press, 1985.

W. Kunz, J. Henle, and B.W. Ninham. 'Zur Lehre von der Wirkung der Salze' (about the science of the effect of salts): Franz Hofmeister's historical papers. *Curr. Opin. Colloid Interface Sci.*, 9:19–37, 2004a.

W. Kunz, P.L. Nostro, and B.W. Ninham. The present state of affairs with Hofmeister effects. *Curr. Opin. Colloid Interface Sci.*, 9:1–18, 2004b.

R. Ladenstein, M. Schneider, R. Huber, K. Wilson, K. Schott, and A. Bacher. Heavy riboflavin synthase from *Bacillus subtilis* crystal structure analysis of the icosahedral β_{60} capsid at 3.3 Å resolution. *J. Mol. Biol.*, 203:1045–1070, 1988.

U.K. Laemmli. Cleavage of structural proteins during the assembly of the head of bacteriophage T4. *Nature*, 227:680–685, 1970.

A. Lomakin, N. Asherie, and G.B. Benedek. Liquid-solid transition in nuclei of protein crystals. *PNAS*, 100(18):10254–10257, 2003.

V. Luzzati and A. Tardieu. Recent developments in solution x-ray scattering. *Ann. Rev. Biophys. Bioeng.*, 9:1–29, 1980.

A.J. Malkin, J. Cheung, and A. McPherson. Crystallization of satellite tobacco mosaic virus I. nucleation phenomena. *J. Cryst. Growth*, 126:544–554, 1993.

A.J. Malkin and A. McPherson. Crystallization, of pumpkin seed globulin: growth and dissolution kinetics. *J. Cryst. Growth*, 133:29–37, 1993a.

A.J. Malkin and A. McPherson. Light scattering investigations of protein and virus crystal growth: ferritin, apoferritin and satellite tobacco mosaic virus. *J. Cryst. Growth*, 128:1232–1235, 1993b.

A.J. Malkin and A. McPherson. Light-scattering investigations of nucleation processes and kinetics of crystallization in macromolecular systems. *Acta Cryst. D*, 50:385–395, 1994.

A.J. Malkin and A. McPherson. Novel mechanisms for defect formation and surface molecular processes in virus crystallization. *J. Phys. Chem. B*, 106: 6718–6722, 2002.

A. McPherson. *Crystallization of Biological Macromolecules.* Cold Spring Harbor Laboratory Press, New York, 1999.

A. McPherson. *Introduction to Macromolecular Crystallography.* Wiley-Liss, 2003.

A. McPherson, Y.G. Kuznetsov, A.J. Malkin, and M. Plomp. Macromolecular crystal growth as revealed by atomic force microscopy. *J. Struct. Biol.*, 142: 32–46, 2003.

A. McPherson, A.J. Malkin, Y.G. Kuznetsov, and S. Koszelak. Incorporation of impurities into macromolecular crystals. *J. Cryst. Growth*, 168:74–92, 1996.

D.A. McQuarrie. *Statistical Mechanics.* University science books, Sausalilto, 2000.

M. Muschol and F. Rosenberger. Interactions in undersaturated and supersaturated lysozyme solutions: Static and dynamic light scattering results. *J. Chem. Phys.*, 103(24):10424–10432, 1995.

M. Muschol and F. Rosenberger. Lack of evidence for prenucleation aggregate formation in lysozyme crystal growth solution. *J. Cryst. Growth*, 167:738–747, 1996.

M. Muschol and F. Rosenberger. Liquid-liquid phase separation in supersaturated lysozyme solutions and associated precipitate formation/crystallization. *J. Chem. Phys.*, 107(6):1953–1962, 1997.

R.R. Netz. Water and ions at interfaces. *Curr. Opin. Colloid Interface Sci.*, 9:192–197, 2004.

N. Niimura, Y. Minezaki, M. Ataka, and T. Katsura. Aggregation in supersatured lysozyme solution studied by time-resolved small angle neutron scattering. *J. Cryst. Growth*, 154:136–144, 1995.

D.W. Oxtoby. Nucleation of first-order phase transition. *Acc. Chem. Res.*, 31: 91–97, 1998.

D.W. Oxtoby. Crystal nucleation in simple and complex fluids. *Philos. T. Roy. Soc. Lond. A*, 361:419–427, 2003.

D.W. Oxtoby and D. Kashchiev. A general relation between the nucleation work and the size of nucleus in multicomponent nucleation. *J. Chem. Phys.*, 100(10):7665–7671, 1994.

V.N. Paunov, E.W. Kaler, S.I. Sandler, and D.N. Petsev. A model for hydration interactions between apoferritin molecules in solution. *J. Col. Int. Sci.*, 240:640–643, 2001.

R. Pecora, editor. *Dynamic Light Scattering: Applications of Photon Correlation Spectroscopy.* Plenum, New York, 1985.

D.N. Petsev, B.R. Thomas, S.-T. Yau, D. Tsekova, C. Nanev, W.W. Wilson, and P.G. Vekilov. Temperature-independent solubility and interactions between apoferritin monomers and dimers in solution. *J. Cryst. Growth*, 232: 21–29, 2001.

D.N. Petsev, B.R. Thomas, S.-T. Yau, and P.G. Vekilov. Interactions and aggregation of apoferritin molecules in solution: Effects of added electrolytes. *Biophys. J.*, 78(4):2060–2069, 2000.

D.N. Petsev and P.G. Vekilov. Evidence for non-dlvo hydration interactions in solutions of the protein apoferritin. *Phys. Rev. Let.*, 84(6):1339–1342, 2000.

R. Piazza. Interactions and phase transitions in protein solutions. *Curr. Opin. Colloid Interface Sci.*, 5:38–43, 2000.

A. Pimpinelli and J. Villain. *Physics of Crystal Growth.* Cambridge University Press, 1998.

J. Poznanski, Y. Georgalis, L. Wehr, W. Saenger, and P. Zielenkiewicz. Comparsion of two different lysozyme types under native and crystallization conditions using two-dimensional NMR and dynamic light scattering. *Biophys. Chem.*, 104:605–616, 2003.

S.W. Provencher. A constrained regularization method for inverting data represented by linear algebraic or integral equations. *Comput. Phys. Comm.*, 27:213–227, 1982a.

S.W. Provencher. Contin: a general purpose constrained regularization program for inverting noisy linear algebraic and integral equations. *Comput. Phys. Comm.*, 27:229–242, 1982b.

P. Retailleau, A. Ducruix, and M. Riès-Kautt. Importance of the nature of anions in lysozyme crystallization correlated with protein net charge variation. *Acta Cryst. D*, 58:1576–1581, 2002.

M.M. Riès-Kautt and A.F. Ducruix. Relative effectiveness of various ions on the solubility and crystal growth of lysozyme. *J. Biol. Chem.*, 264(2):745–748, 1989.

L. Rodriguez-Fernández. *Crystallization of lumazine synthase from* Bacillus subtilis*: electron microscopic observations*. PhD thesis, Technische Universität München, 2003.

D. Roessner. *White paper refractive index increment*. Wyatt Technology Europe GmbH, 1996.

D.F. Rosenbaum and C.F. Zukoski. Protein interactions and crystallization. *J. Cryst. Growth*, 169:752–758, 1996.

F. Rosenberger, P.G. Vekilov, M. Muschol, and B.R. Thomas. Nucleation and crystallization of globular proteins — what we know and what is missing. *J. Cryst. Growth*, 168:1–27, 1996.

A. Sali, R. Glaeser, T. Earnest, and W. Baumeister. From words to literature in structural genomics. *Nature*, 422:216–225, 2003.

K.S. Schmitz. *An Introduction to Dynamic Light Scattering by Macromolecules*. Academic Press, New York, 1990.

K. Schott, R. Ladenstein, A. König, and A. Bacher. The lumazine synthase-riboflavin synthase complex of *Bacillus subtilis*. *J. Biol. Chem.*, 265(21): 12686–12689, 1990.

R.P. Sear. Heterogeneous nucleation near a metastable vapor-liquid transition: the effect of wetting transition. *J. Phys.: Condens. Matter*, 14:3693–3703, 2002.

M. Shah, O. Galkin, and P.G. Vekilov. Smooth transition from metastability to instability in phase separating protein solutions. *jcp*, 121:7505–7512, 2004.

A. Stradner, H. Sedgwick, F. Cardineaux, W.C.K. Poon, S. Egelhaaf, and P. Schurtenberger. Equilibrium cluster formation in concentrated protein solutions and colloids. *Nature*, 432:492–495, 2004.

D.I. Svergun, S. Richards, M.H.J. Koch, Z. Sayers, S. Kuprin, and G. Zaccai. Protein hydration in solution: Experimental observation by x-ray and neutron scattering. *Proc. Natl. Acad. Sci. USA*, 95:2267–2272, 1998.

J. Tack. *Elektronenmikroskopische Untersuchungen zur Defektstruktur und zum Wachstumsmechanismus von Proteinkristallen*. PhD thesis, Technische Universität München, 1997.

J. Tack, N. Braun, and S. Weinkauf. Electron microscopy of protein crystal growth. *Europ. J. Cell Biol.*, 74:32–32, 1997.

S. Tanaka, K. Ito, R. Hayakawa, and M. Ataka. Size and number density of precrystalline aggregates in lysozyme crystallization process. *J. Chem. Phys.*, 111(22):10330–10337, 1999.

Z. Tavassoli and R. P. Sear. Homogeneous nucleation near a second phase transition and ostwald's step rule. *J. Chem. Phys.*, 116(12):5066–5072, 2002.

P.R. ten Wolde and D. Frenkel. Enhancement of protein crystal nucleation by critical density fluctuations. *Science*, 277:1975–1978, 1997.

B. R. Thomas, D. Carter, and F. Rosenberger. Effect of microheterogeneity on horse spleen apoferritin crystallization. *J. Cryst. Growth*, 187:499–510, 1998.

P. Umbach, Y. Georgalis, and W. Saenger. Time-resolved small-angle light scattering on lysozyme during nucleation and growth. *J. Am. Chem. Soc.*, 120:2382–2390, 1998.

P.G. Vekilov and A.A. Chernov. *Solid State Physics*, volume 57, chapter The physics of protein crystallization, pages 1–147. Academic Press, 2002.

P.G. Vekilov and F. Rosenberger. Intrinsic kinetics flucutations as cause of growth inhomogeneity in protein crystals. *Phys. Rev. E*, 57:6979–6981, 1998.

O.D. Velev, E.W. Kaler, and A.M. Lenhoff. Protein interactions in solution characterized by light and neutron scattering: comparison of lysozyme and chymotrypsinogen. *Biophys. J.*, 75:2682–2697, 1998.

G.A. Vliegenthart and H.N.W. Lekkerker. Predicting the gas-liquid critical point from the second virial coefficient. *J. Chem. Phys.*, 112(12):5364–5369, 2000.

W.W. Wilson. Light scattering as a diagnostic for protein crystal growth - A practical approach. *J. Struct. Biol.*, 142:56–65, 2003.

S.-T. Yau, D.N. Petsev, B.R. Thomas, and P.G. Vekilov. Molecular-level thermodynamic and kinetic parameters for the self-assembly of apoferritin molecules into crystals. *J. Mol. Biol.*, 303:667–678, 2000.

S.-T. Yau and P.G. Vekilov. Quasi-planar nucleus structure in apoferritin crystallization. *Nature*, 406:494–497, 2000.

A.C. Yin, Y. Inatomi, N.I. Wakayama, and W.D. Huang. Measurement of temperature and concentration dependences of refractive index of hen-egg-white lysozyme solution. *Cryst. Res. Technol.*, 38(9):785–792, 2003.

T.-S. Yoon, S. Tetreault, H.E. Bosshard, R.M. Sweet, and J. Sygusch. Mosaic spread analysis of Canadian advanced protein crystallization experiment on the Russian space station Mir. *J. Cryst. Growth*, 232:520–535, 2001.

B.H. Zimm. The scattering of light and the radial distribution function of high polymer solutions. *J. Chem. Phys.*, 16(12):1093–1099, 1948.